NASA
Technical Memorandum 80132

AVRADCOM
Technical Report 79-41

Wind-Tunnel Investigation of an Armed Mini Remotely Piloted Vehicle

Arthur E. Phelps III

SEPTEMBER 1979

NASA

U.S. ARMY AVRADCOM

NASA
Technical Memorandum 80132

AVRADCOM
Technical Report 79-41

Wind-Tunnel Investigation of an Armed Mini Remotely Piloted Vehicle

Arthur E. Phelps III
Structures Laboratory, AVRADCOM Research and Technology Laboratories
Langley Research Center
Hampton, Virginia

National Aeronautics
and Space Administration

**Scientific and Technical
Information Branch**

1979

SUMMARY

A wind-tunnel investigation of a full-scale remotely piloted vehicle (RPV) armed with rocket launchers has been conducted in the Langley V/STOL tunnel. The longitudinal, lateral, and directional aerodynamic characteristics of the vehicle were determined for both powered and unpowered conditions. In addition, the aerodynamic control power of the control surfaces was evaluated.

The results of the test indicate that the model had unacceptable longitudinal stability characteristics at negative angles of attack in the original design configuration. The addition of a pair of fins mounted in a V-arrangement on the propeller shroud resulted in a configuration with acceptable longitudinal stability characteristics. The addition of wing-mounted external stores to the modified configuration resulted in a slight reduction in the longitudinal stability.

The lateral-directional characteristics of the model were generally good, but the model had low directional stability at low angles of attack, such as might be encountered in a strike-dive maneuver. Aerodynamic control power was very strong around all three axes, though there was a small degradation in aileron control power at high positive angles of attack.

INTRODUCTION

During the decade of the 1970's, the U.S. Army has developed a strong interest in the use of the small remotely piloted vehicle (hereinafter referred to as mini-RPV) for use in intelligence-gathering missions in excessively hostile battlefield environments. A fairly recent development program has led to the production and deployment of the XMQM-105 Aquila reconnaisance mini-RPV on a trial basis (see ref. 1), and work is currently under way on new applications of this concept. One possible application involves the use of rocket launchers on the wings of the reconnaisance RPV's in order to provide an extremely low-risk, long-range strike capability which would be under the direct control of the local battlefield commander.

As part of a continuing effort to direct and evaluate original applications of the RPV concept, the U.S. Army AVRADCOM Research and Technology Laboratories have established contract programs with private industry to design and flight-test armed mini-RPV's of a type similar to the XMQM-105.

Flight-testing of an armed mini-RPV of this type and weight (swept-wing, pusher-propeller, 890 N (200 lbf)) has never been done, so the present investigation was conducted in the Langley V/STOL tunnel at the request of the U.S. Army in order to provide some indication of the flight characteristics of such a configuration. The vehicle was a modified R-4D Sky Eye mini-RPV and was tested with power on and power off over a range of angle of attack from negative to positive stall for both the armed and unarmed configurations.

In addition, a series of tests was run to define the aerodynamic control power of the aerodynamic control surfaces, and the effectiveness of wing-mounted dive brakes was determined.

SYMBOLS

All data in this report are referred to the stability axis system shown in figure 1. The moment center was located on the fuselage reference line at a point corresponding to the design center-of-gravity position of 19 percent of the mean aerodynamic chord. Measurements and calculations were made in U.S. Customary Units and are presented in the International System of Units (SI) with the U.S. Customary Units given parenthetically. Physical constants relating the two systems of units used in this paper may be obtained from reference 2.

b	wing span, 3.71 m (12.17 ft)
C_D	drag coefficient, D/qS
C_L	lift coefficient, L/qS
C_l	rolling-moment coefficient, M_X/qSb
C_{l_β}	dihedral parameter, $\partial C_l/\partial\beta$
$C_{l_{\delta_a}}$	aileron effectiveness, $\partial C_l/\partial\delta_a$
C_m	pitching-moment coefficient, $M_Y/qS\bar{c}$
$C_{m_{\delta_e}}$	elevator effectiveness, $\partial C_m/\partial\delta_e$
C_n	yawing-moment coefficient, M_Z/qSb
$C_{n_{\delta_r}}$	rudder effectiveness, $\partial C_n/\partial\delta_r$
C_T	thrust coefficient, T/qS
C_Y	side-force coefficient, F_Y/qS
$\bar{c}$	mean aerodynamic chord, 0.81 m (2.66 ft)
D	drag, N (lb)
F_A	axial force, N (lb)
F_N	normal force, N (lb)
F_Y	side force, N (lb)
L	lift, N (lb)

M_X rolling moment, m-N (in-lb)

M_Y pitching moment, m-N (in-lb)

M_Z yawing moment, m-N (in-lb)

q free-stream dynamic pressure, Pa (lb/ft^2)

R Reynolds number based on mean aerodynamic chord

S reference wing area, 2.805 m^2 (30.188 ft^2)

T effective thrust (drag with propeller removed minus drag with propeller operating), N (lb)

V free-stream velocity, m/sec (ft/sec)

α angle of attack of fuselage reference line, deg

β angle of sideslip of model center line, deg

δ_a aileron deflection (right aileron), positive for trailing edge down, deg

$\delta_{d.b.}$ dive-brake deflection, deg

δ_e elevator deflection (symmetric right and left aileron), positive trailing edge up, deg

δ_r rudder deflection, positive trailing edge right, deg

MODEL AND APPARATUS

Static force and moment tests were conducted in the Langley V/STOL tunnel using the full-scale flight vehicle shown in figure 2. The major components of the model were constructed of a very lightweight, rigid, aramid-fiber, honeycomb composite which had been laid up in female molds, and secondary structural components were built from foam-filled fiberglass reinforced plastic shells. Propulsive power for the model was provided by a 63.50-cm (25.0-in.) pusher propeller driven by a two-cylinder, two-stroke-cycle, 220 cc gasoline engine which developed approximately 11.2 kW (15 hp) at 7000 revolutions per minute (rpm). Fuel was supplied to the engine from a tank mounted below the test section and pressurized with nitrogen in such a manner as to lift the fuel to the level of the carburetors. The engine was mounted to the rear of the short, box-shaped fuselage, and a shroud supported by three struts attached to the engine cowling surrounded the propeller.

The shroud was not intended to be a propeller duct in the classical sense, but it was incorporated both as a safety feature and as a guard to protect the propeller from damage during recovery operations. The primary reason that the shroud could not be used as a duct concerned the vibration characteristics of

the engine. During start-up and shutdown, there was substantial engine vibration, and soft rubber shock mounts were used to isolate heavy vibratory loads from the fuselage. As a result, there was considerable lateral motion of the engine and propeller in the shroud, and that motion prohibited the use of close tip clearance required by an efficient duct arrangement. A full-length rudder for directional control was hinged to fittings attached on the top and bottom of the shroud.

The trailing edge of the wing was equipped with ailerons extending from the middle of the wing semispan outboard to the wing tip. Longitudinal control was obtained by symmetric deflections of the two ailerons, and roll control was provided by asymmetric deflection of the ailerons. Dive brakes were fitted to the trailing edge of the wing between the aileron and propeller shroud and were deflected symmetrically as shown in figure 2. All control surfaces, as well as the engine throttle, were controlled remotely using flight-type servo mechanisms actuated by a control box in the tunnel control room.

During the test program, a number of modifications to the basic configuration were developed and tested in an effort to modify some adverse aerodynamic characteristics which were discovered during preliminary screening tests. These modifications included a V-tail arrangement attached to the propeller shroud, swept-drooped wing tips, and both large and small nose strakes attached to the fuselage at the leading edge of the wing-fuselage juncture. Details of the various modifications are presented in figures 2(b) and 2(c).

Two different types of rocket launchers were tested on the model and are shown in figure 3(a). The first type of launcher was a twin-tube configuration for launching standard 2.75-in. (6.99-cm) rockets, and the second type of launcher was designed to carry seven antiarmor VIPER rockets in seven tubes clustered in a cylindrical arrangement. The launcher for the 2.75-in. rockets used standard launch tubes fabricated into an integral launcher pylon assembly bolted to hard points on the wing, and the VIPER launcher was simulated by an aluminum and wood cylinder of the proper dimensions. A drag-reduction cowling of the type reported in reference 3 was fabricated from fiberglass and attached to the front face of the VIPER launcher for some tests. Figure 3(b) shows the size and location of a hemispherical reconnaisance dome used for some tests.

TESTS AND CORRECTIONS

The investigation was conducted in the 4.42-m (14.5-ft) by 6.63-m (21.75-ft) test section of the Langley V/STOL tunnel with the model strut-mounted on a six-component strain-gage internal balance. (See fig. 4.) The majority of the test was conducted at a free-stream dynamic pressure of 718 Pa (15 lb/ft^2) for a Reynolds number of 1.904×10^6 based on the mean aerodynamic chord. In order to evaluate the effect of Reynolds number on the aerodynamic characteristics of the model in the low-speed regime, some tests were run over a range of dynamic pressure from 239 Pa (5 lb/ft^2) to 718 Pa (15 lb/ft^2) for a Reynolds number range of 1.1×10^6 to 1.9×10^6.

Longitudinal aerodynamic characteristics were obtained by sweeping the model through an angle-of-attack range from -18° to the positive stall angle of attack at zero sideslip, and lateral-directional characteristics were obtained by sweeping the model through a sideslip range of -10° to 10° at angles of attack of -12°, 0°, and 12°.

During powered testing, the following procedure was used to obtain the desired thrust coefficient:

Cruise C_T: The tunnel airspeed was brought up to the desired level, and model angle of attack was adjusted to produce the design lift coefficient of 0.50. Engine speed was then adjusted to produce $C_D = 0$, and minor adjustments were made to both the angle of attack and engine rotational speed to obtain $C_L = 0.5$ and $C_D = 0$. The resulting engine rotational speed was then held constant through either an angle-of-attack sweep or an angle-of-sideslip sweep.

Climb C_T: The tunnel airspeed was brought up to the desired level, and the engine was run up either to its redline speed of 8500 rpm or to full throttle, whichever condition occurred first for the airspeed under study. During the angle-of-attack or angle-of-sideslip sweep, power was held either at full throttle or 8500 rpm, whichever was the appropriate limit.

Idle C_T: The tunnel airspeed was brought up to the desired level, and engine speed was maintained at the design idle speed of 3500 rpm.

Control powers of the aerodynamic control surfaces were determined by remotely sweeping the controls through a range of deflections at selected angles of attack, angles of sideslip, and airspeeds.

PRESENTATION OF RESULTS

The results of this wind-tunnel investigation are presented in coefficient form in figures 5 to 28, according to the following format:

RESULTS AND DISCUSSION

Basic Longitudinal Aerodynamic Characteristics

The basic longitudinal aerodynamic characteristics of the model are presented in figures 5 to 7. Figure 5 presents the longitudinal aerodynamics of the model over a range of Reynolds number with all gaps sealed and the engine cooling inlets sealed and faired. The data show very little sensitivity to Reynolds number except for the negative maximum lift coefficient, which is of little importance in the mission of this class of vehicle. Figure 6(a) presents a comparison of the longitudinal aerodynamics of the fully sealed configuration with those of the flight configuration, and figure 6(b) is a comparison of the drag characteristics for three configurations: fully sealed, sealed with cooling air inlets open (control-surface gaps and all joints sealed and faired), and no seals (flight configuration). The data indicate that the cooling drag penalty was fairly low, approximately 5 percent of minimum C_D, but gap drag was very high at 17 percent of the minimum C_D. Since this was a prototype flight article, this very high gap drag may not be representative of the drag to be expected on production vehicles.

Figure 7 shows the longitudinal aerodynamics of the basic vehicle, along with those for the case with the propeller shroud removed and for the case with both the propeller shroud and the engine cowling removed. (With the cowling removed, the engine and muffler, along with the engine controls, were exposed

to the airstream.) As was expected, the most significant effects were seen in the pitching-moment curve, but what was surprising was that the cowling, not the propeller shroud, had the greatest effect on longitudinal stability, especially at low angles of attack. A series of flow-visualization studies and exploratory tests showed that the two upper-shroud support struts (see figs. 2(a) and 2(b)) were acting as a small, delta-shaped horizontal tail. At positive angles of attack, the struts were immersed in the wing-root flow and were washed by a vortex from the lip of the cooling inlet duct; thus, they were transparent to the free-stream flow. At negative angles of attack, however, the struts became exposed to the free stream, and, though small and inefficient when compared with a typical horizontal tail, did provide some measure of stability.

The low longitudinal stability for this wing-body combination at low and negative angles of attack is typical for a high-wing configuration and is primarily a result of fuselage-wing interference. Preliminary aerodynamic screening tests showed that there was a region of unstable flow in the wing-body juncture which grew progressively more severe with increasing negative angle of attack. In an effort to reduce the adverse flow interaction in the wing-body juncture, strakes were attached to the leading edge of the wing root forward along the side of the nose. The intention was to generate a stationary vortex to stabilize the flow in the wing-body juncture, but the data of figure 8 indicate that neither the small strakes nor the large strakes which were tested were effective in improving the longitudinal stability, and that the large strakes were actually destabilizing.

A series of tests were run with a pair of swept and drooped wing tips which were designed primarily to improve the lateral-directional characteristics of the model, and the effects of these tips on the longitudinal aerodynamics are shown in figure 5. The tips increased both the span and area of the wing and shifted the aerodynamic center farther aft on the fuselage. The change in the pitching-moment data of figure 9 was almost entirely a pure rotation of the curve due to an overall increase in static margin, rather than an alteration of the basic aerodynamic characteristics. A careful examination of the two pitching-moment coefficient curves of figure 9 shows that both curves, although different in slope, have the same shape, which indicates that the basic aerodynamic characteristics remain basically unchanged.

Since the armed mini-RPV is essentially a weapons delivery system, a high degree of stability over a wide range of vehicle attitudes is important for accurate aiming. Furthermore, high stability should be obtained by altering the basic configuration as little as possible in order to ensure the maximum compatibility between the XMQM-105 Aquila mini-RPV now in use by the U.S. Army and the final strike vehicle. Thus, considerable effort was expended in an attempt to find a solution to the low-angle-of-attack longitudinal instability apart from the addition of stabilizing surfaces which might interfere with current launcher systems.

A series of further exploratory tests were run to establish the feasibility of using vortex generators, fairings, or a combination of both fairings and vortex generators to alter the wing root flow. The results, which are not reported here, showed virtually no effect on the longitudinal aerodynamics.

Finally, a pair of fins was mounted on the propeller shroud in a V-arrangement (see fig. 2(b)) so as to provide both longitudinal and directional stability. The longitudinal aerodynamics of the model with the duct fins are presented in figure 10(a).

The data of figure 10(a) show that the duct fins tended to straighten out the portion of the pitching-moment curve at negative lift coefficients and that there was a slight rotation of the curve toward a greater stability margin. While this effect was admittedly small, there was nevertheless a change in both the slope and the shape of the pitching-moment coefficient curve.

The effects of external stores on the longitudinal aerodynamic characteristics are shown in figures 11 to 13. The data of figure 11 show that the reconnaisance dome was destabilizing at low lift coefficients for the basic configuration (fig. 11(a)), but with the dive brakes deployed, the stability was approximately the same as for the clean basic configuration (fig. 11(b)). As a general observation, it was noted that the model configurations with the dive brakes deployed were always more stable longitudinally than the same configurations with the dive brakes retracted. Flow surveys around the inboard end of the deflected dive brake showed that a strong vortex was shed from the upper inboard corner of the dive-brake leading edge and that this vortex swept the upper surface of the upper-shroud support struts in such a way as to increase their efficiency. The positive increment in the pitching-moment coefficient of figure 11(a) is the result of the drag increment of the drag brakes acting above the model center of gravity. The addition of the duct fins to the configuration with the reconnaisance dome resulted in a configuration which was longitudinally stable over the entire angle-of-attack range.

Figure 12 presents longitudinal data for the model with the twin-tube 2.75-in. rocket launchers attached. Drag data are shown in figure 12(b) for both the loaded and empty launchers in order to provide a comparison of the drag penalties for the two launcher conditions. Apart from the drag increment associated with the launcher, there was no significant effect of the launchers on the longitudinal aerodynamics.

Figure 13 presents a comparison of longitudinal data for the model with the 2.75-in. rocket launchers, the VIPER launchers, and the modified VIPER launchers. The most obvious effect of the launchers was, of course, on the drag (fig. 13(b)), but there was also a slight lift loss imposed by the unmodified VIPER launchers. Figure 13(b) shows that the drag of the VIPER launcher fitted with the ring cowl was, for moderate positive lift coefficients, actually slightly lower than the drag of the 2.75-in. launchers at the same lift coefficients.

The effects of power on the longitudinal aerodynamic characteristics of the model are shown in figures 14 to 16. Figure 14 presents the aerodynamic characteristics for power off, cruise power, and maximum power for the clean model with duct fins. The most significant characteristic of the data is that there was virtually no effect of power on the longitudinal stability. The data have been resolved about the design center-of-gravity location; therefore, there should be no longitudinal trim changes with power for the flight condition. There was, however, a slight increase in negative lift at negative angle

of attack, probably due to the slightly improved flow characteristics over the inboard portion of the wing as a result of the flow velocities induced by the propeller. Figure 15 presents power-on and power-off longitudinal data for the fully loaded model (reconnaisance dome and two 2.75-in. launchers). With power on, there was a small increase in longitudinal stability at negative lift coefficients and a small increase in negative lift capability, but in general, there was no significant effect of power on the loaded configuration. Figure 16 presents the effect of dive brakes on the longitudinal characteristics of the model with cruise power and shows an increase in the longitudinal stability as was the case with the unpowered model.

Lateral-Directional Aerodynamic Characteristics

The lateral-directional characteristics of the basic configuration are shown in figure 17 for three angles of attack. As expected, the model exhibited positive dihedral effect $\left(\text{negative } C_{l_\beta}\right)$ at positive angles of attack, and negative dihedral effect at negative angles of attack. The directional stability was generally very low $\left(C_{l_\beta} = 0.0006/\text{deg}\right)$ and was not significantly affected by angle of attack. Figure 18 presents the lateral-directional characteristics of the model with the duct fins and shows a slight increase in directional stability due to the tail $\left(C_{l_\beta} = 0.00075/\text{deg}\right)$ and a decrease in the dihedral effect.

One desirable characteristic for the strike mission was to have $C_{l_\beta} = 0$ at very low lift coefficients. This neutral dihedral effect would permit lateral adjustments in the aiming of the missiles during an attack dive maneuver without inducing rolling moments during aiming. The data of figures 17 and 18(a) show that at $C_L = 0$, the model had $C_{l_\beta} \approx -0.007/\text{deg}$ for the basic configuration, and $C_{l_\beta} \approx -0.004/\text{deg}$ for the model with the duct fins. A pair of drooped and swept wing tips were tested, as discussed previously, in an effort to reduce the dihedral effect at $C_L = 0$, and the results are shown in figure 18(b). The data of figure 18(b) show that for the model with the drooped tips, $C_{l_\beta} \approx -0.0035/\text{deg}$ at $C_L = 0$, and that the reduction in C_{l_β} occurred at the higher angles of attack where the wing was more heavily loaded. For this reason, the drooped tips were not incorporated into the modified configuration (basic configuration plus duct fins).

The lateral-directional characteristics of the model with the reconnaisance dome and the 2.75-in. rocket launchers are shown in figures 19 and 20, respectively. In general, the data show a slight decrease in the directional stability for both configurations when compared with the clean configurations of figures 17 and 18. In addition, there was some loss in dihedral effect at negative angles of attack for the configuration with the 2.75-in. launchers, but there was still positive dihedral effect (though small) at $\alpha = 0^\circ$. Figure 21 presents the lateral-directional characteristics for the fully loaded

configuration (reconnaisance dome and 2.75-in. launcher) and shows a significant loss in directional stability at low and negative angles of attack when compared with the basic configuration. Small fins were mounted at the bottom aft end of the launchers as shown in figure 3(a). The data of figure 21(b) show improved directional stability for the launcher-fin configuration at $\alpha = 0^{\circ}$, although the directional stability characteristics at $\alpha = -12^{\circ}$ remain poor. The configuration with the VIPER launcher had fairly good lateral-directional characteristics as shown by the data of figure 22.

Figure 23 shows the lateral-directional characteristics of the model at $\alpha = 0^{\circ}$ for power off, cruise power, and cruise power with dive brakes deflected. The data show that power caused a modest increase in the dihedral effect but had virtually no effect on directional stability. Deflecting the dive brakes reduced the directional stability slightly and increased the dihedral effect by a small amount.

Control Power

The results of a series of tests to define the control power of the aerodynamic control surfaces are presented in figures 24 to 26 for pitching-moment coefficient versus elevator deflection, rolling-moment coefficient versus aileron deflection, and yawing-moment coefficient versus rudder deflection. The moment coefficient data have been adjusted by the moments at zero control deflection in order to remove the offsets so that control power slopes may be compared directly without the effects of geometric asymmetries. The data of figures 24 to 26 have been summarized as control derivatives $C_{m_{\delta_e}}$, $C_{l_{\delta_a}}$, and $C_{n_{\delta_r}}$ versus angle of attack for two sideslip conditions in figures 27(a) and 27(b), and figure 28 shows the effect of thrust coefficient on the directional control power.

In general, the control data show that there was considerable control power around all axes and that the ailerons lost effectiveness with increasing angle of attack, but both the rudder and elevator remained essentially unaffected by α. Deflecting the dive brakes caused a reduction in the elevator and aileron effectiveness, primarily as a result of the highly unstable flow at the inboard end of the control surfaces. As expected, the directional control power increased with increasing thrust coefficient.

CONCLUSIONS

A modified R-4D Sky Eye mini-RPV was tested in the Langley V/STOL tunnel. The vehicle had a 3.71-m (12.17-ft) wing span, and was tested both with power on and power off over a range of angle of attack from negative to positive stall for both armed and unarmed configurations. In addition, a series of tests were run to define the aerodynamic control power of the aerodynamic control surfaces, and the effectiveness of wing-mounted dive brakes was determined. The major results of this investigation are summarized as follows:

1. The model had unacceptable longitudinal stability characteristics at negative angles of attack in the design configuration. The addition of a pair of fins mounted in a V-arrangement on the propeller shroud resulted in a configuration with acceptable longitudinal stability characteristics over the entire angle-of-attack range.

2. The addition of wing-mounted external stores to the modified configuration resulted in a slight reduction in the longitudinal stability.

3. Deflection of partial-span, wing-mounted dive brakes produced a large increment in drag, and provided a beneficial increment in longitudinal stability for all configurations tested.

4. The lateral-directional characteristics of the model were generally good, but the model had low directional stability at low angles of attack such as might be encountered in a strike dive maneuver.

5. Increasing thrust coefficient caused a slight increase in longitudinal stability for the fully loaded configuration (reconnaisance dome and two 2.75-in. rocket launchers) and a slight increase in positive dihedral effect. There were no adverse effects of power on the aerodynamic characteristics of the model.

6. Aerodynamic control power was very powerful around all three axes, though there was a small degradation in aileron control power at high positive angles of attack.

7. The high aerodynamic drag coefficient of the large cylindrical VIPER launcher has been reduced to a level below that for the standard 2.75-in. launcher by using a ring cowl mounted to the front face of the VIPER launcher.

Langley Research Center
National Aeronautics and Space Administration
Hampton, VA 23665
August 2, 1979

REFERENCES

1. RPV System Test Report - Aerodynamics. LMSC-L028081 (Contract DAAJ02-75-C-0005), Lockheed Missiles & Space Co., May 1977.

2. Standard for Metric Practice. E 380-76, American Soc. Testing & Mater., 1976.

3. Phelps, Arthur E., III; and Wilson, John C.: Wind-Tunnel Investigation of Three Rocket Launcher Systems. NASA TM SX-78763 (AVRADCOM TR 78-44), 1978.

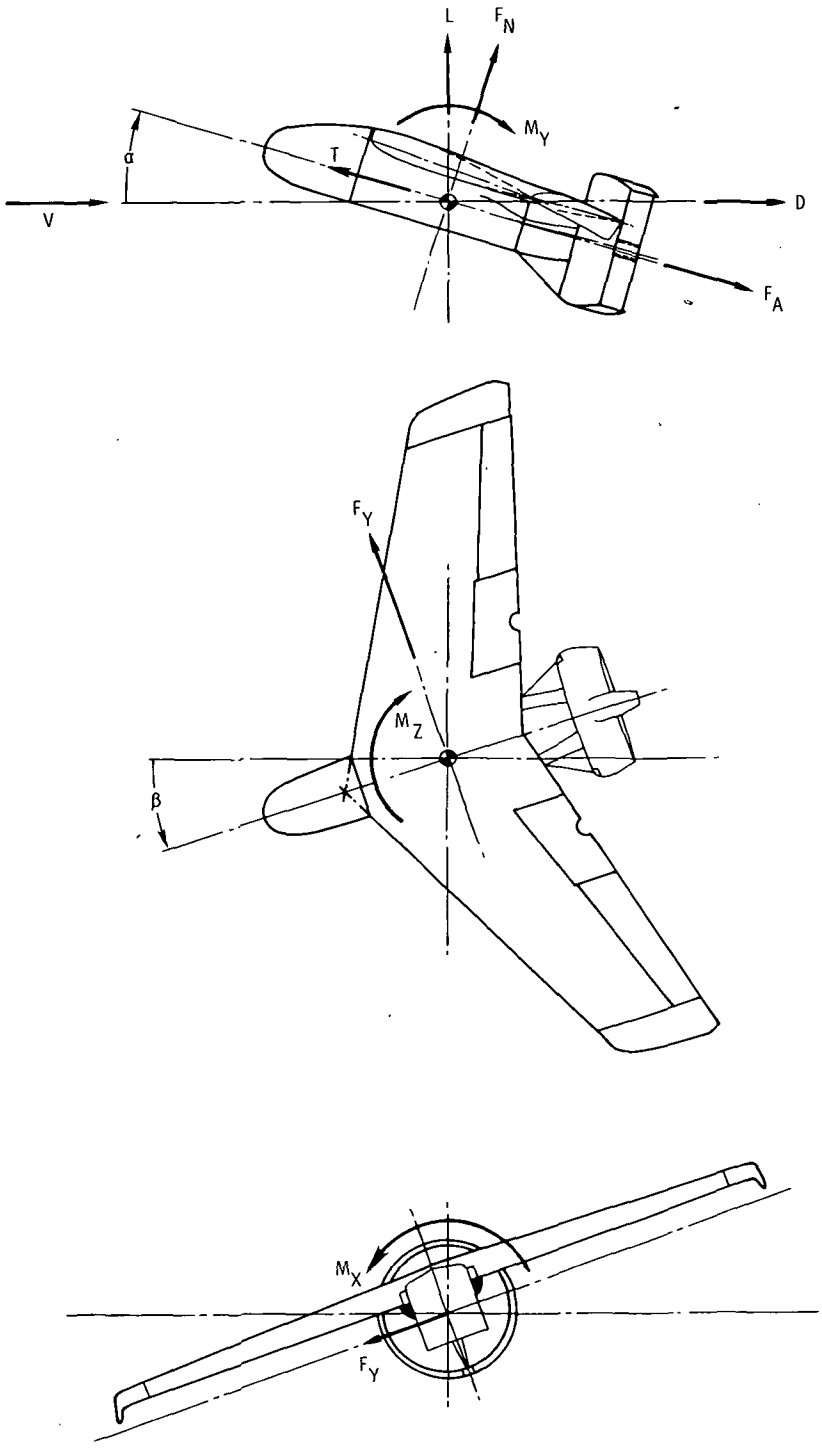

Figure 1.- Axis system used in presentation of data. Arrows denote positive direction of forces, moments, and angular displacements.

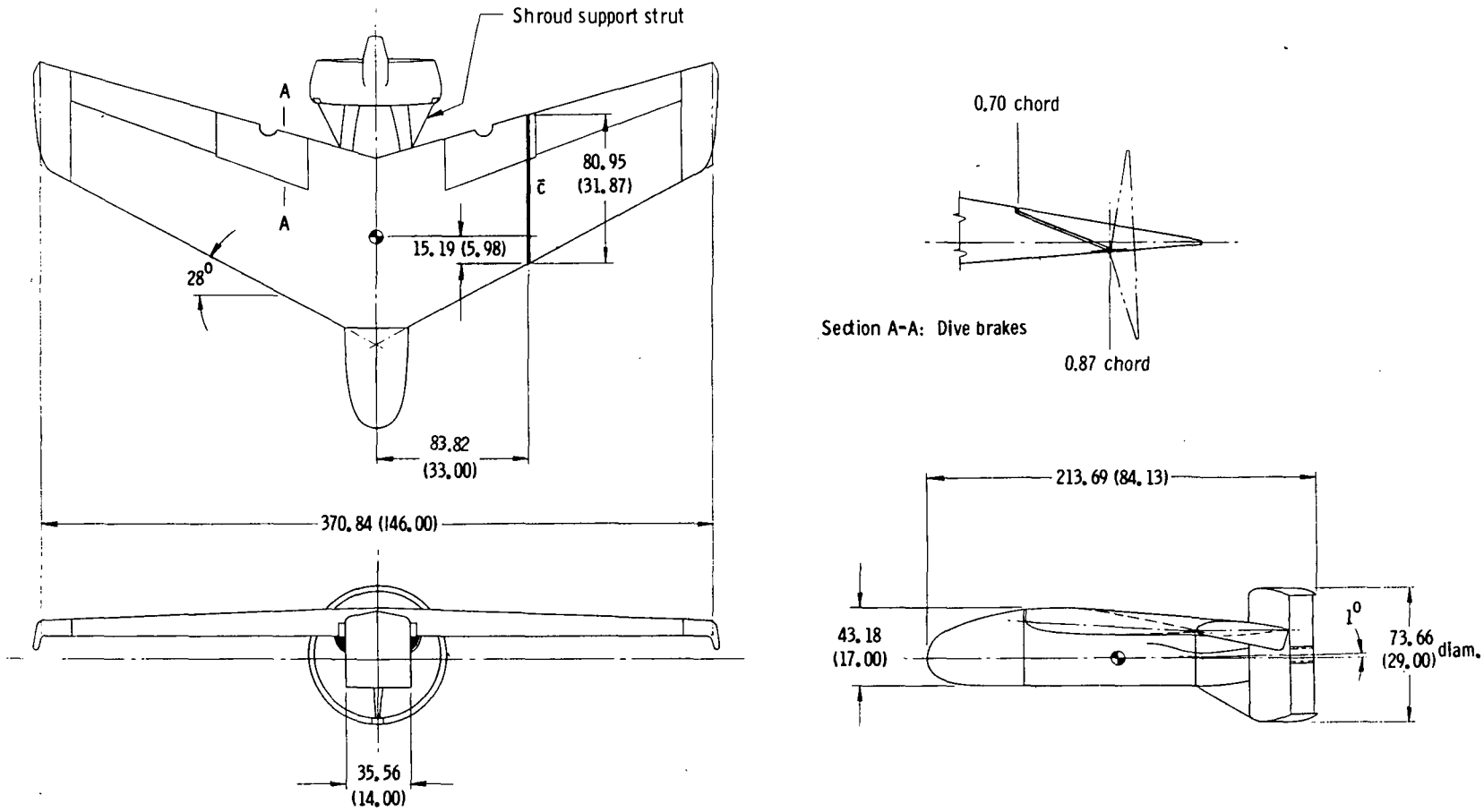

(a) General arrangement.

Figure 2.- Details of model. All linear dimensions given in cm (in.).

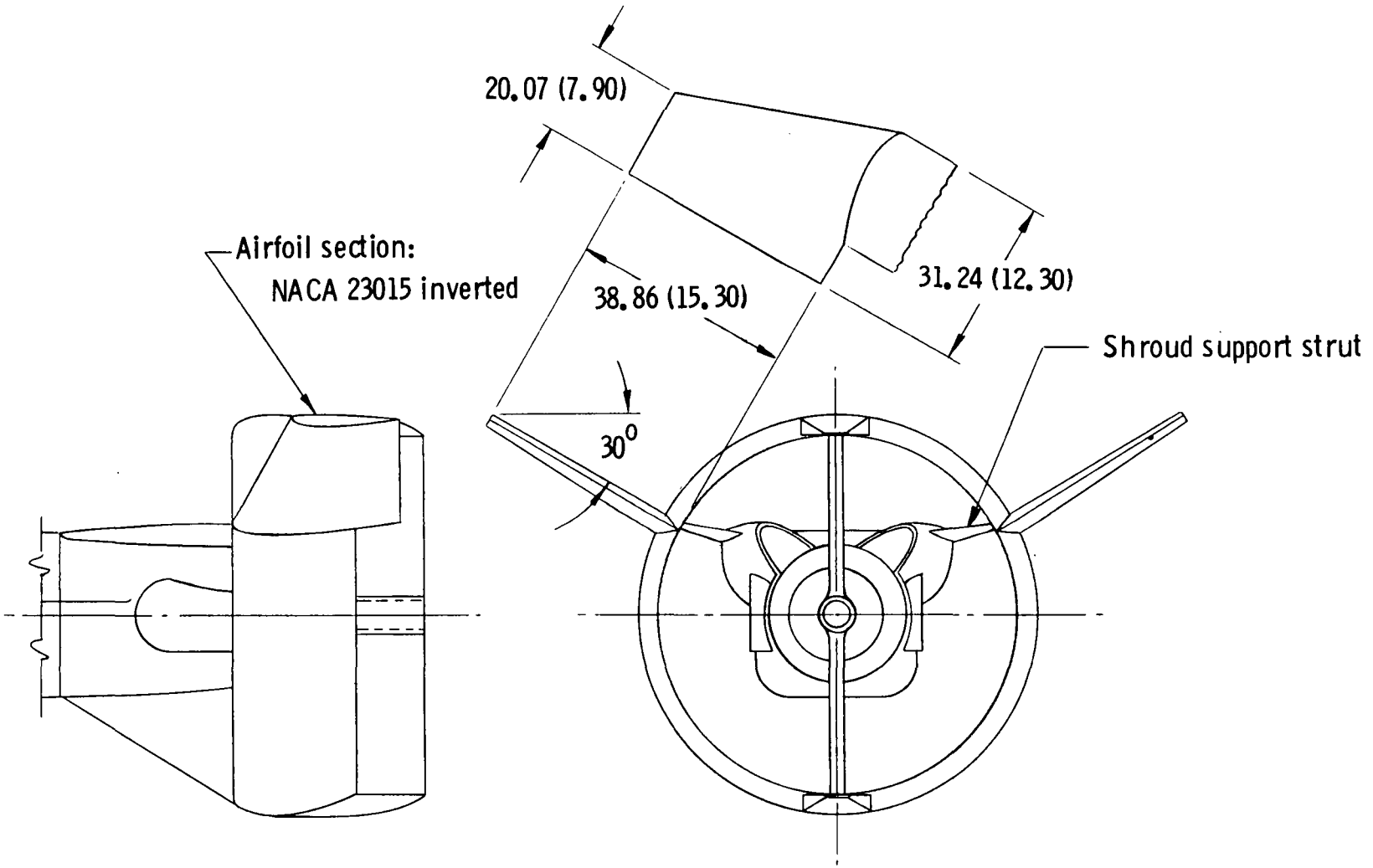

(b) Details of modifications.

Figure 2.- Continued.

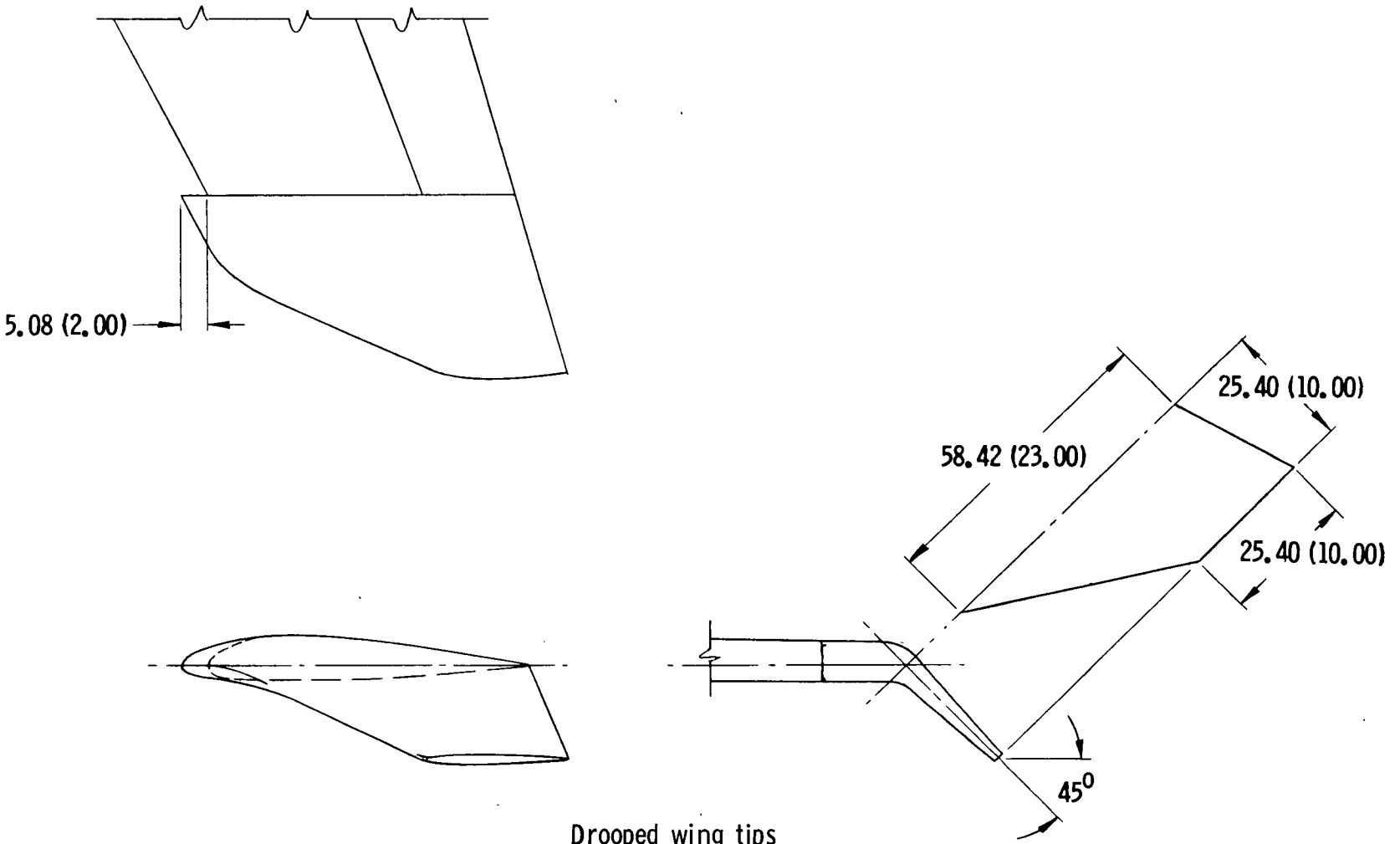

Drooped wing tips

(b) Concluded.

Figure 2.- Continued.

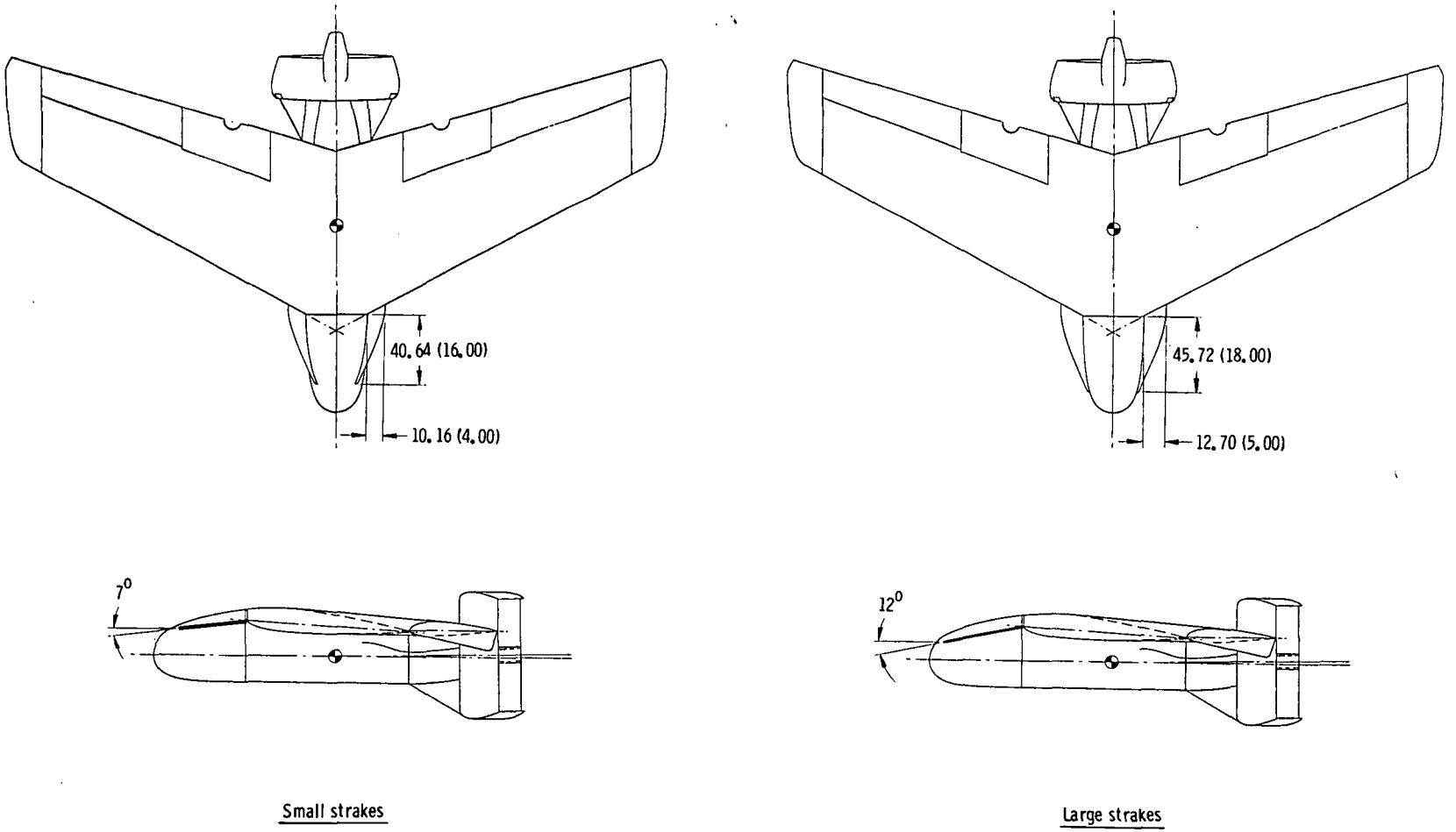

(c) Nose strakes.

Figure 2.- Concluded.

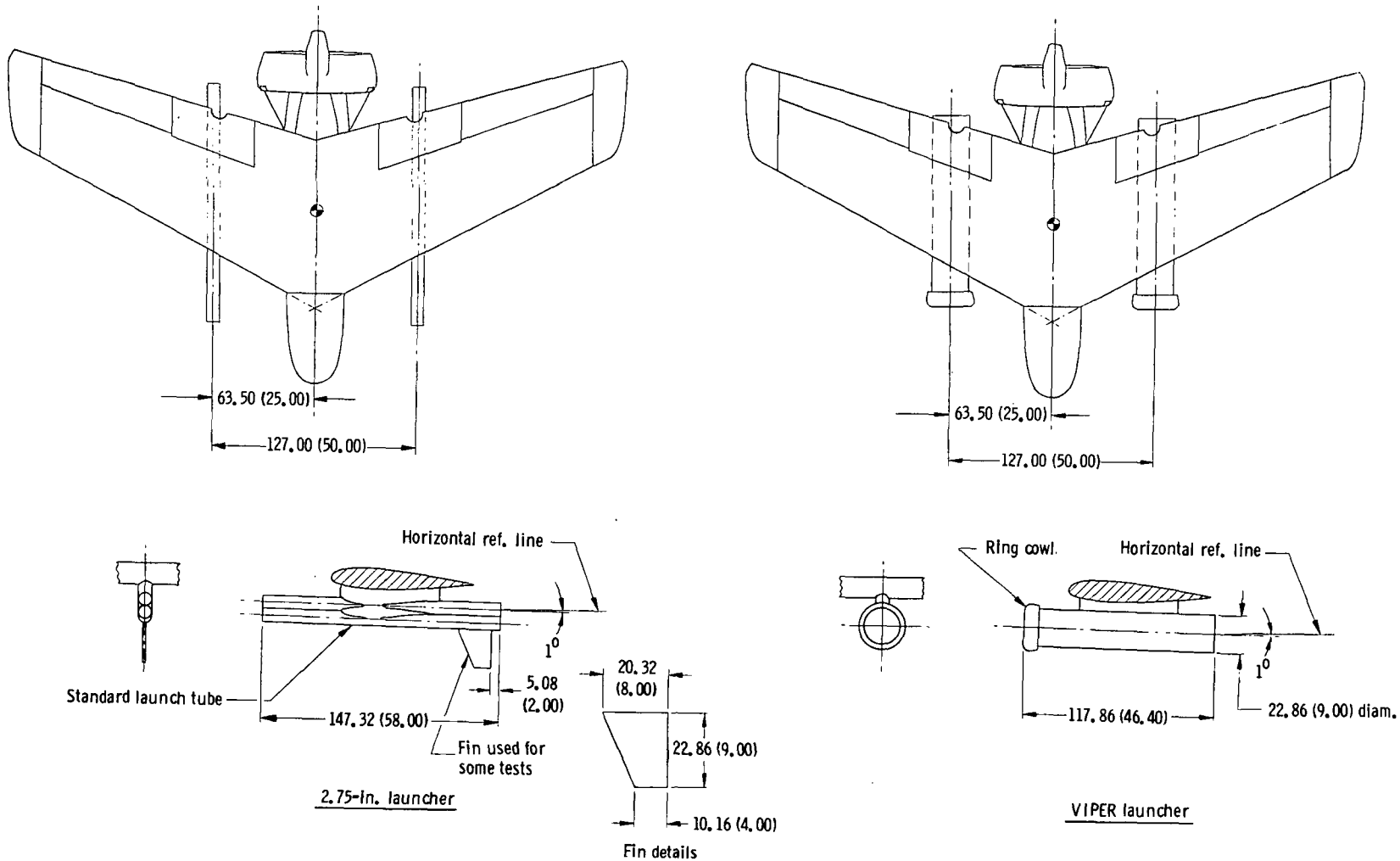

(a) Rocket launchers.

Figure 3.- External stores. All linear dimensions given in cm (in.).

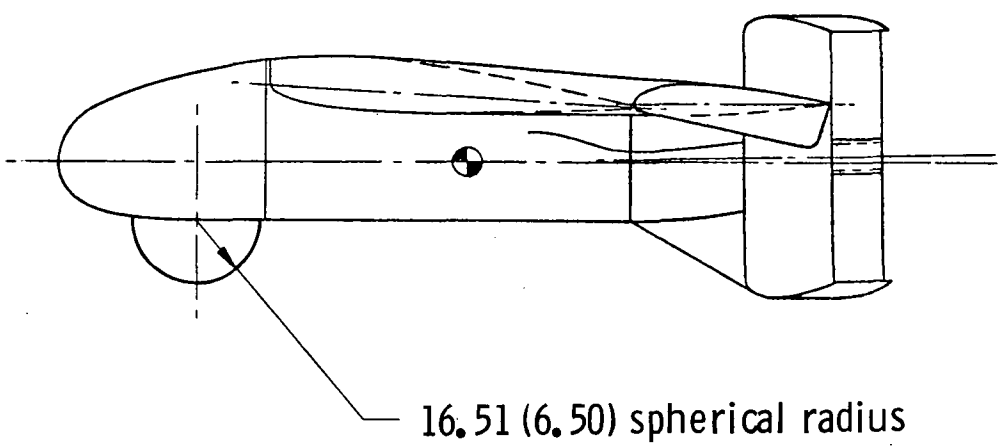

(b) Reconnaisance dome.

Figure 3.- Concluded.

L-78-8350

Figure 4.- Photograph of model in Langley V/STOL tunnel.

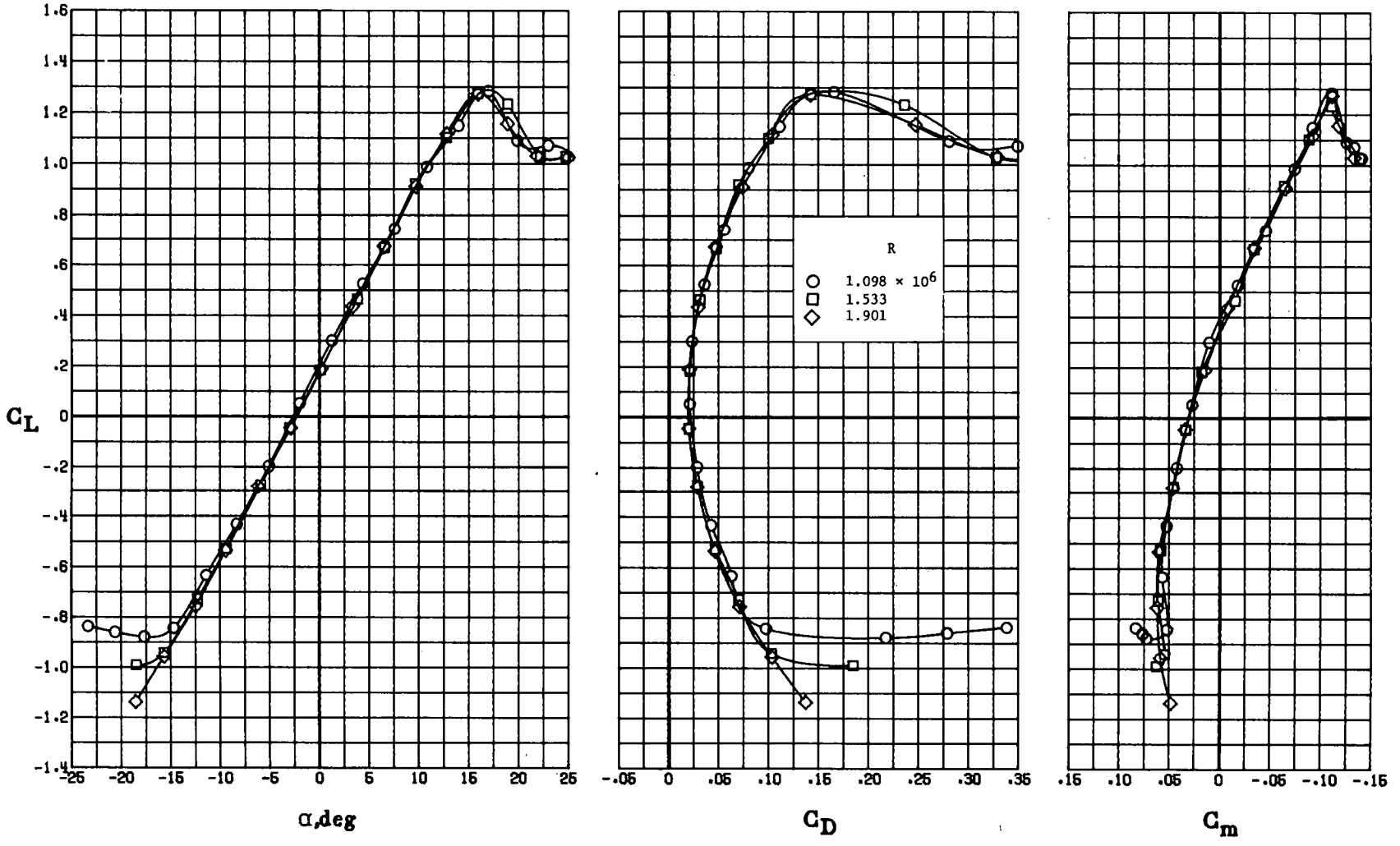

Figure 5.- Effect of airspeed on longitudinal aerodynamic characteristics of model in basic configuration. Propeller off; model sealed.

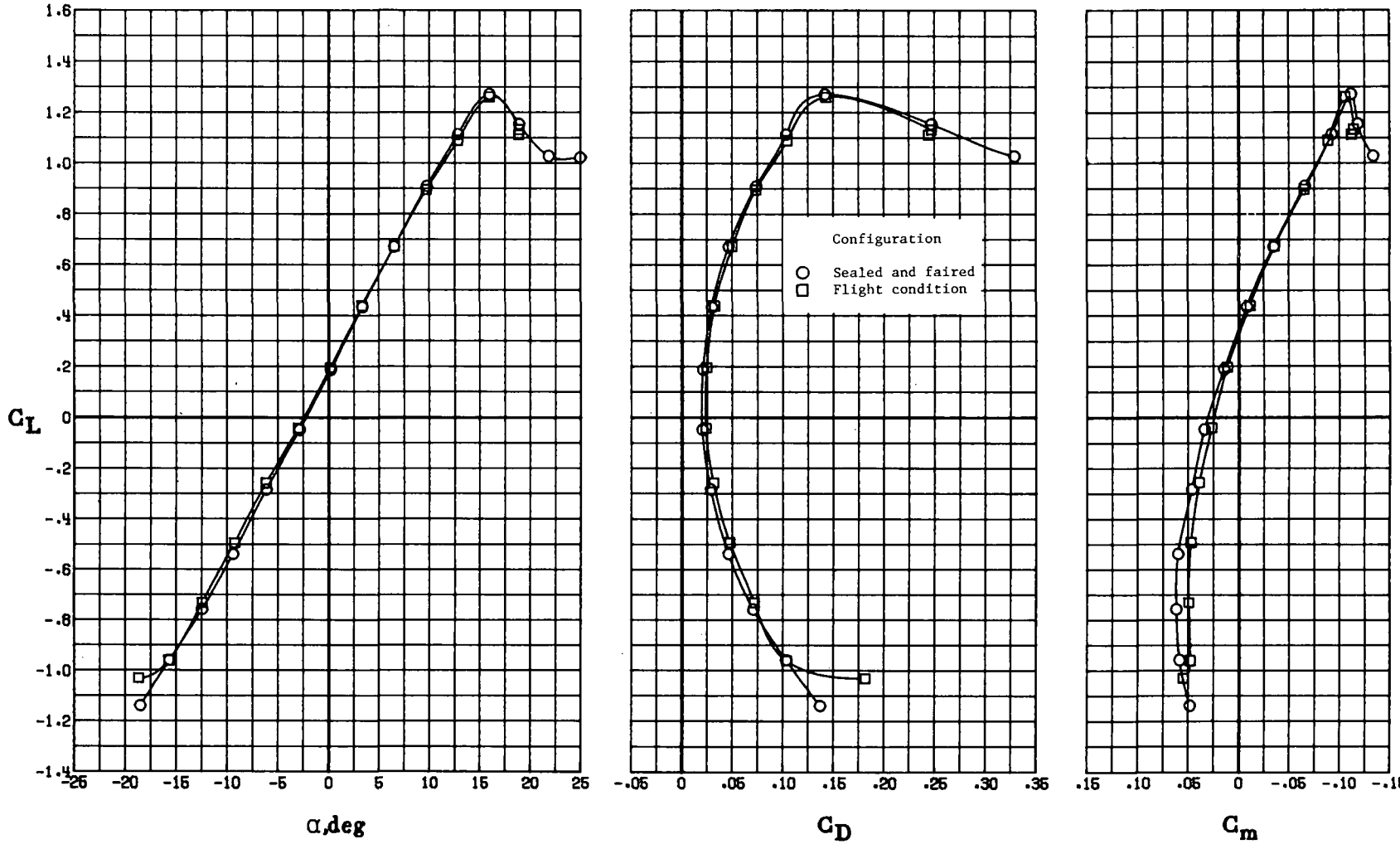

(a) Overall longitudinal characteristics.

Figure 6.- Effect of seals on longitudinal aerodynamic characteristics of model in basic configuration. Propeller off.

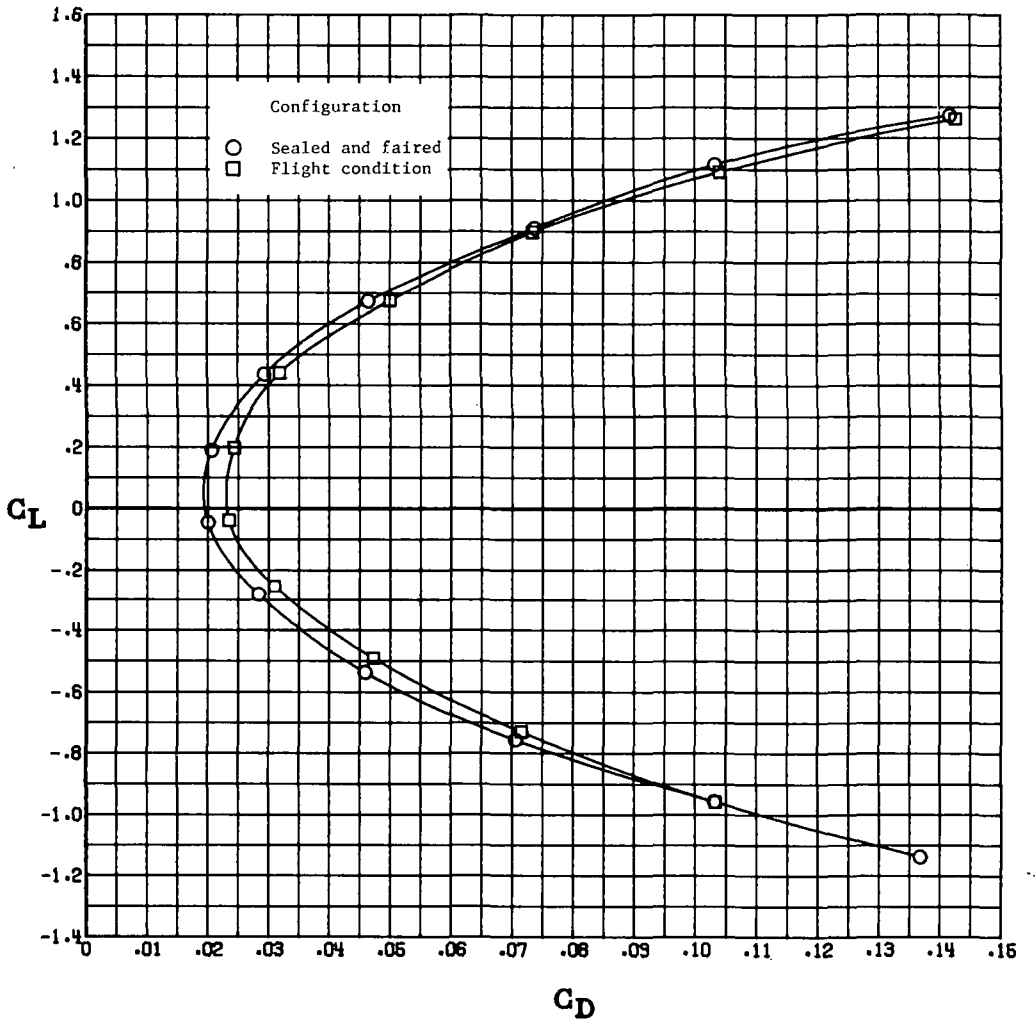

(b) Drag characteristics.

Figure 6.- Concluded.

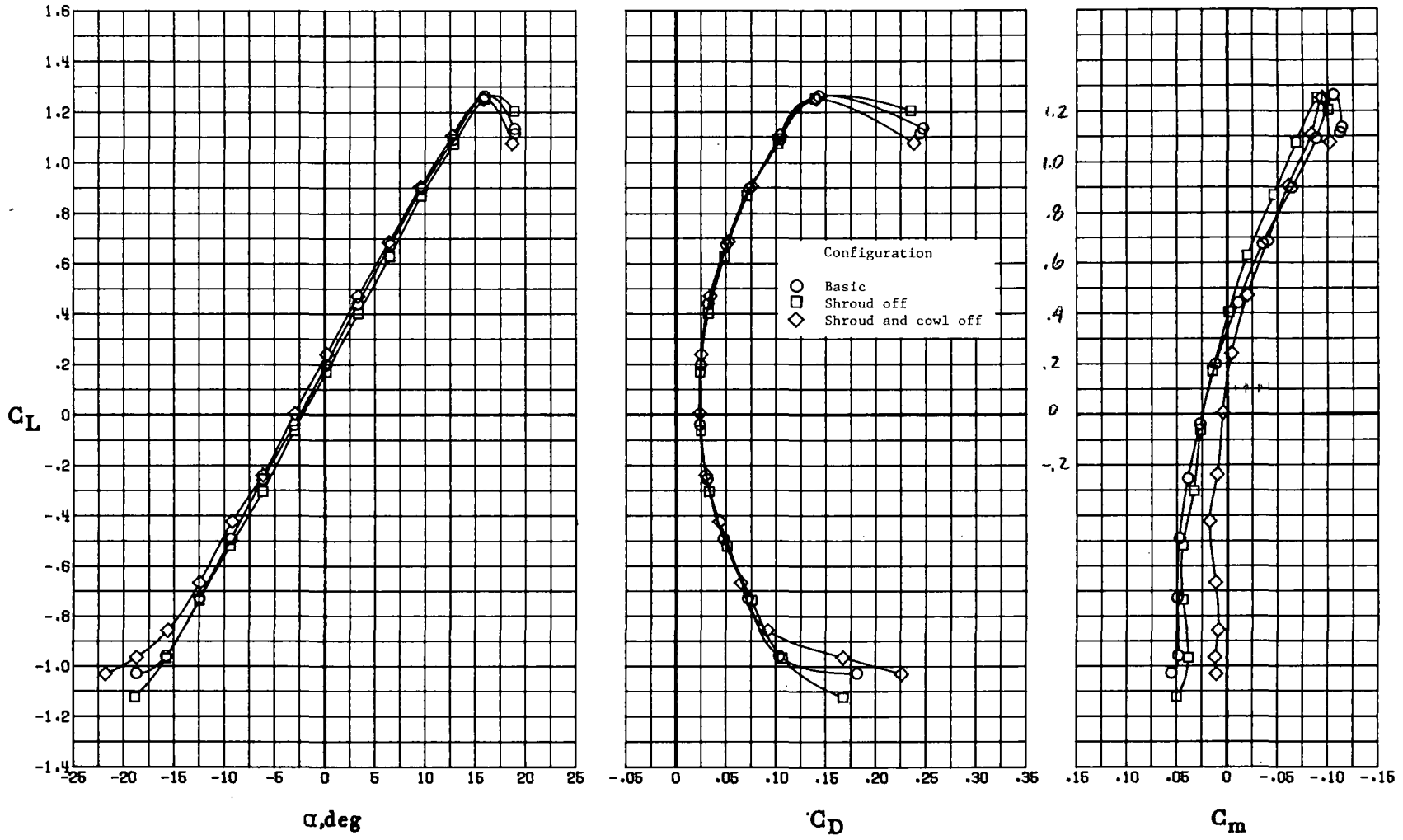

(a) Overall longitudinal characteristics.

Figure 7.- Effect of engine cowling and propeller shroud on longitudinal aerodynamic characteristics of model in basic configuration. Propeller off.

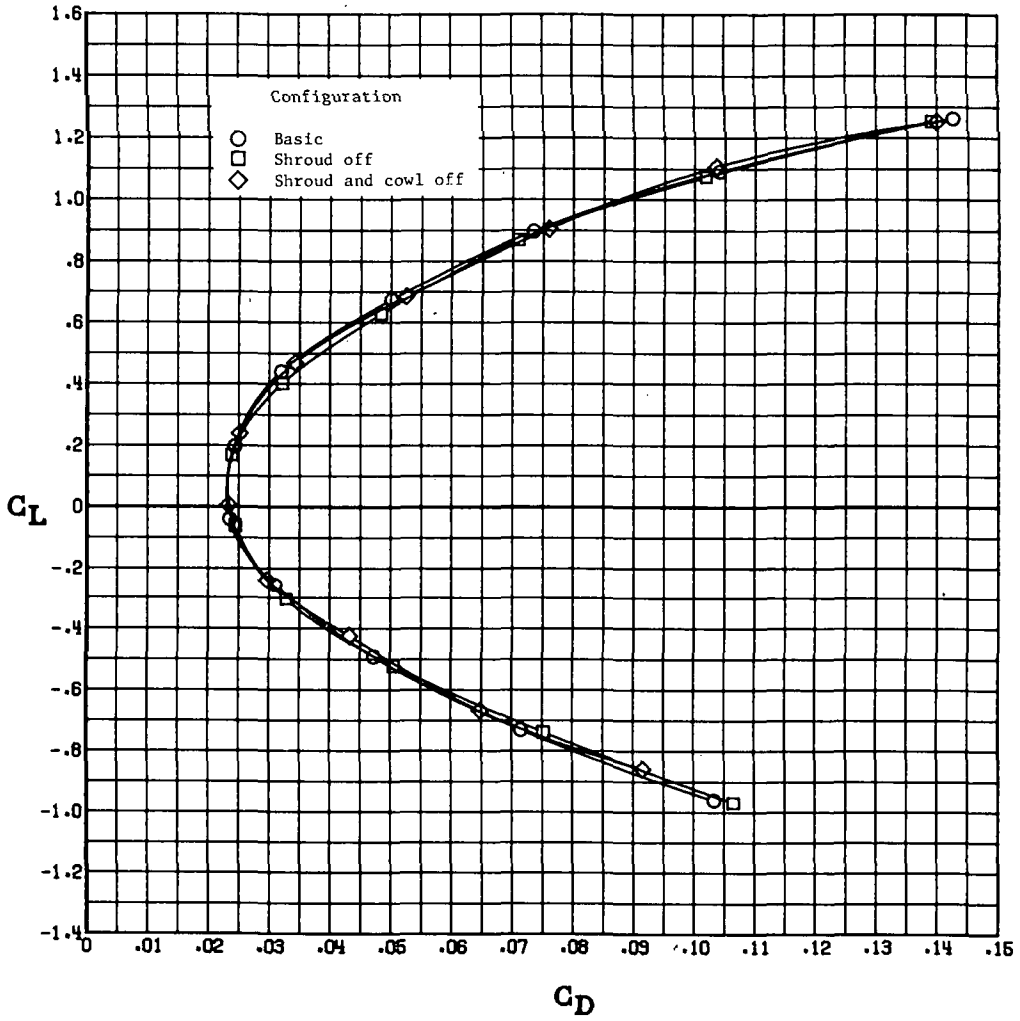

(b) Drag characteristics.

Figure 7.- Concluded.

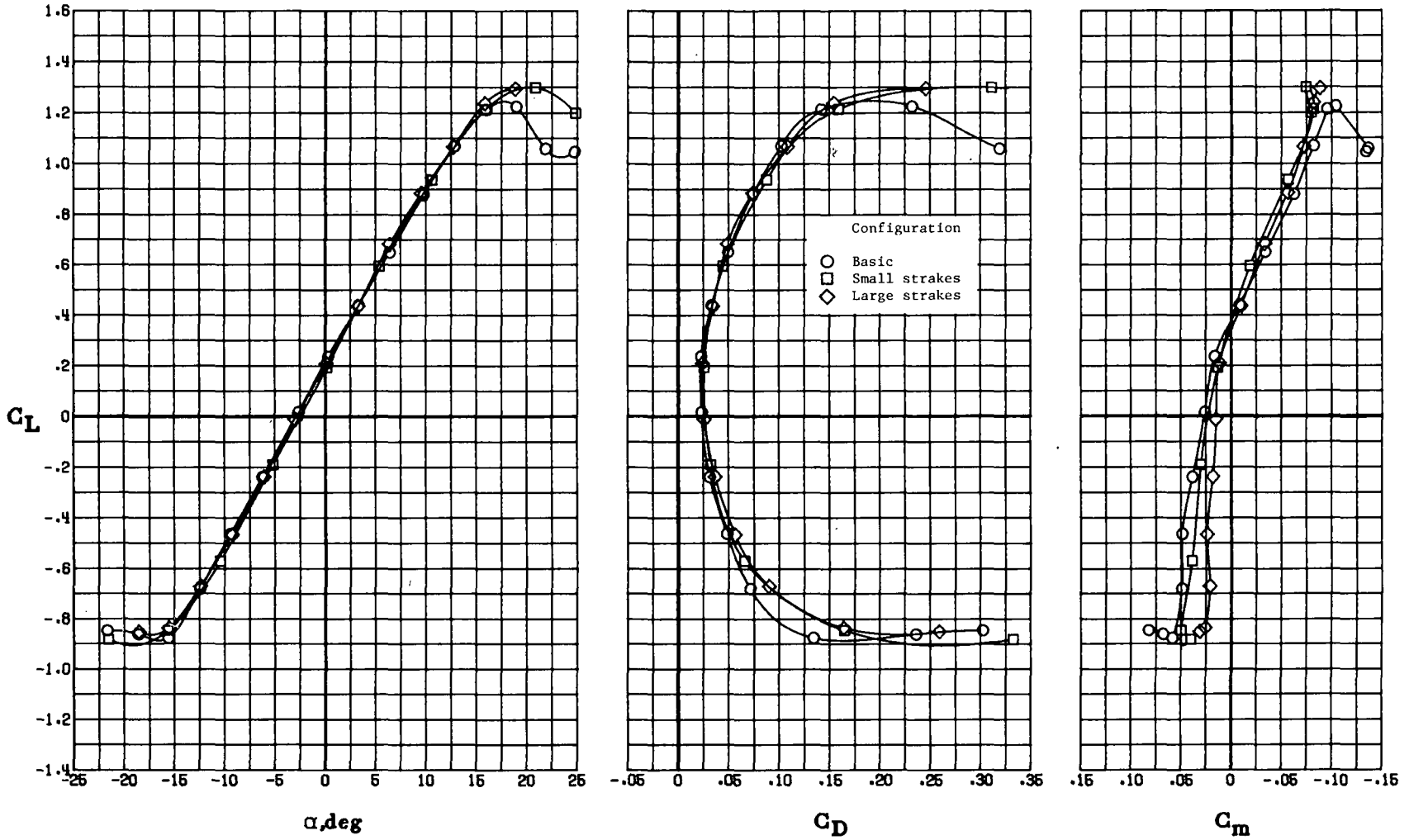

Figure 8.- Effect of strakes on longitudinal aerodynamic characteristics of model in basic configuration. Propeller off.

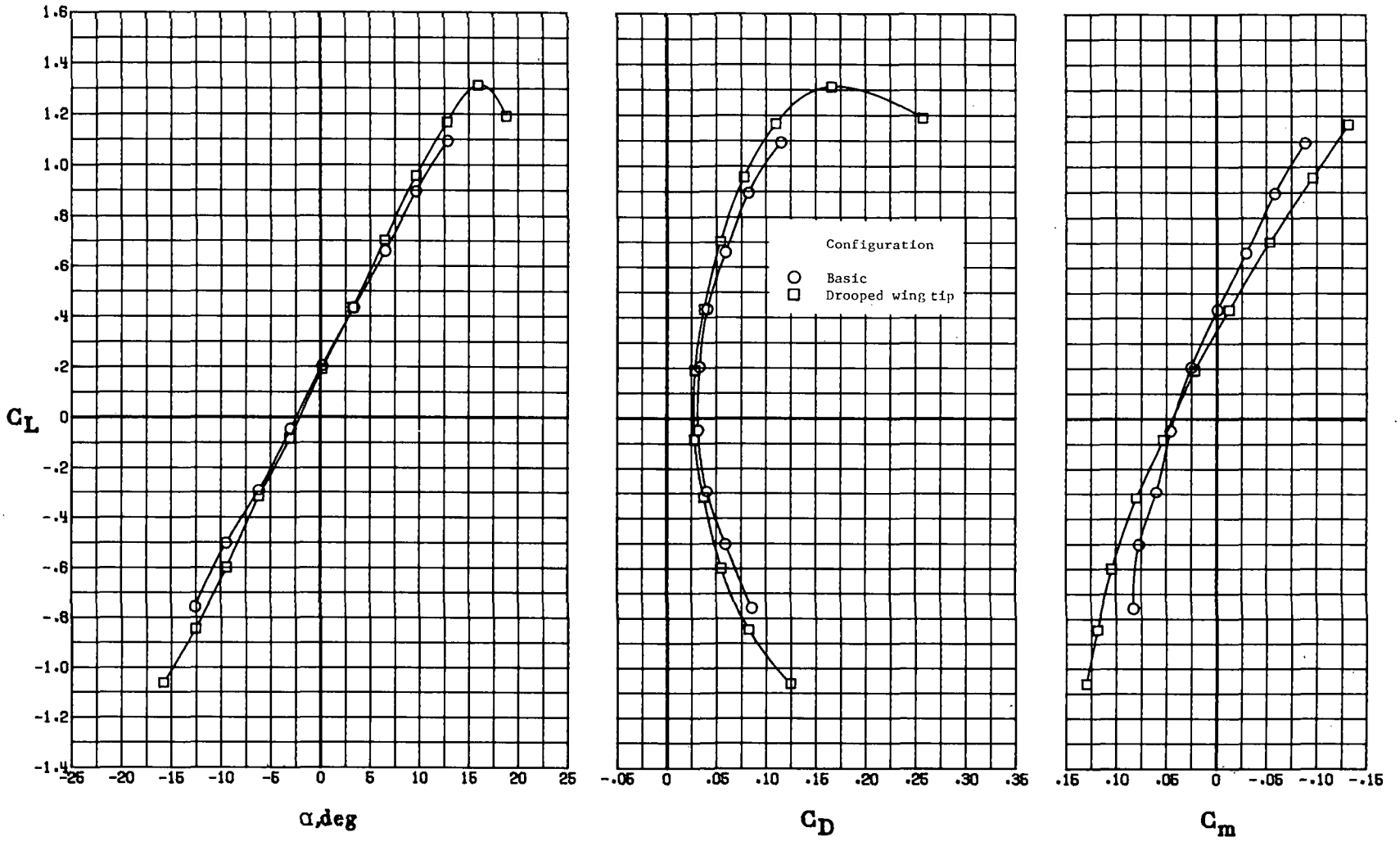

Figure 9.- Effect of drooped wing tips on longitudinal aerodynamic characteristics of model in basic configuration. Propeller off.

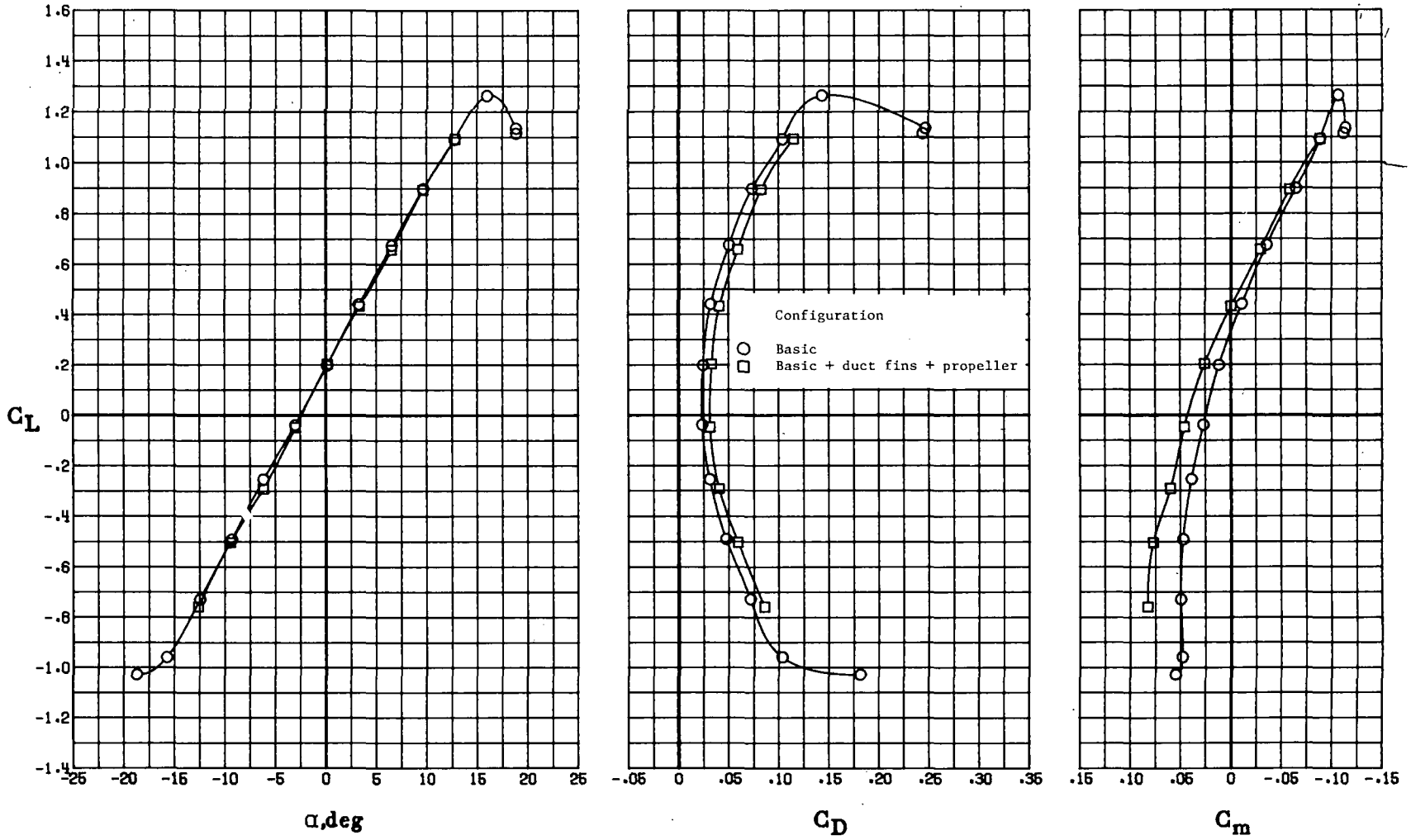

(a) Overall longitudinal characteristics.

Figure 10.- Effect of duct fins on longitudinal aerodynamic characteristics of model in basic configuration.

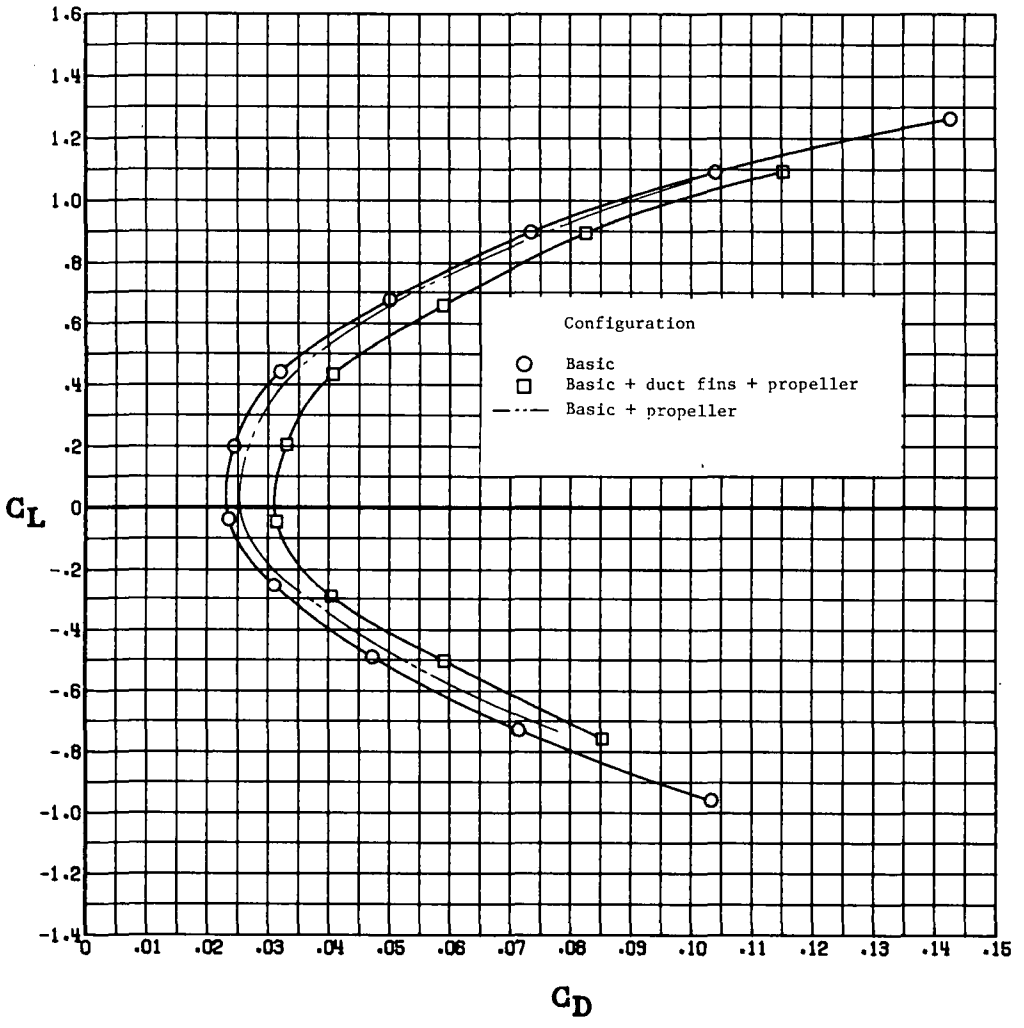

(b) Drag characteristics.

Figure 10.- Concluded.

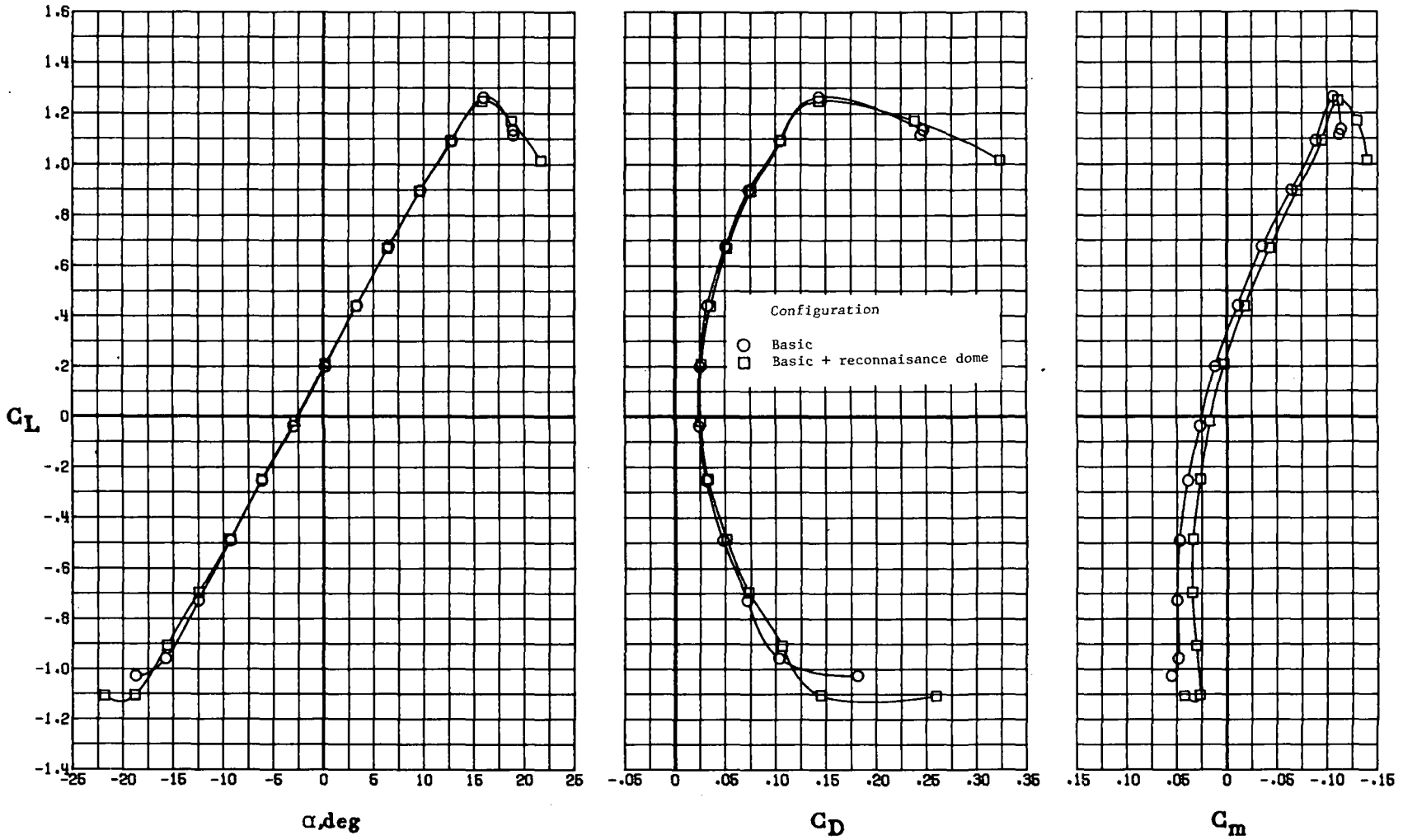

(a) Effect of reconnaisance dome on overall longitudinal characteristics.

Figure 11.- Longitudinal aerodynamic characteristics of model with reconnaisance dome.

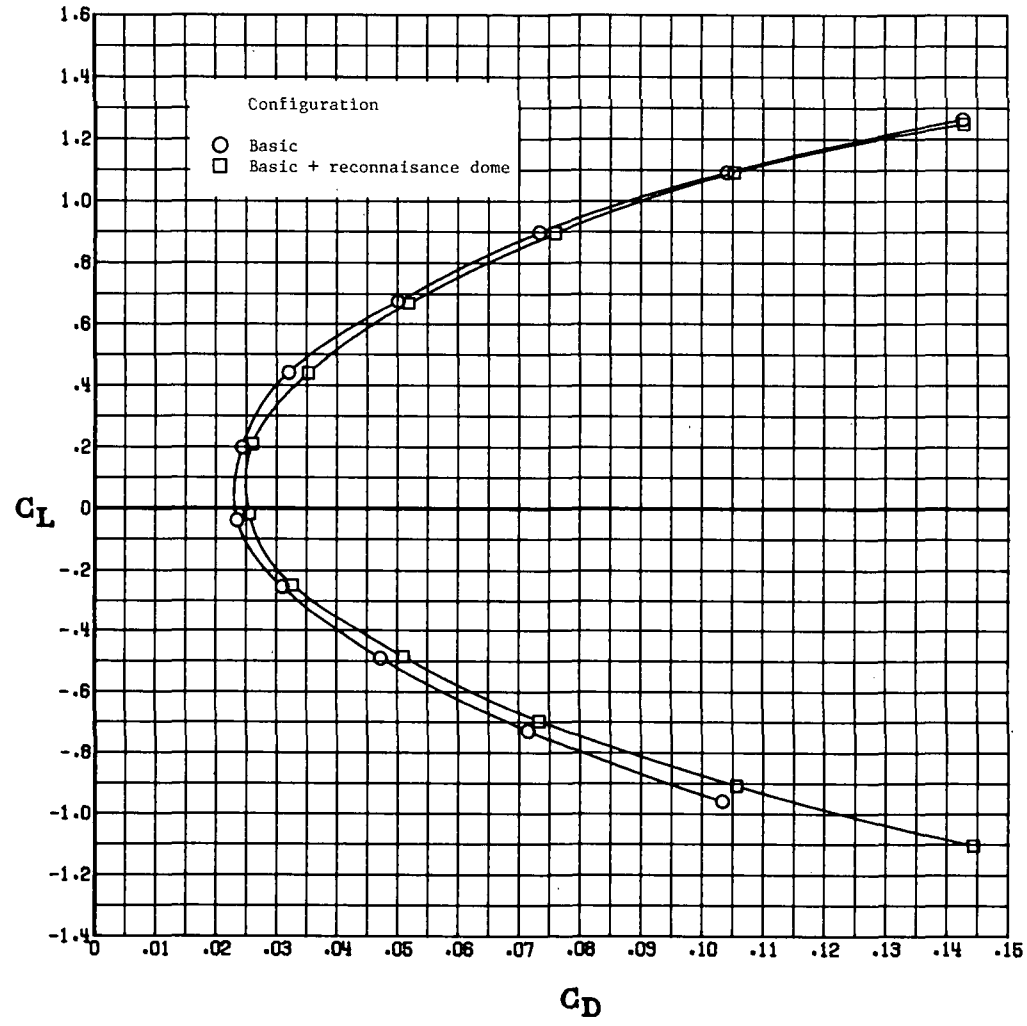

(b) Effect of reconnaisance dome on drag characteristics.

Figure 11.- Continued.

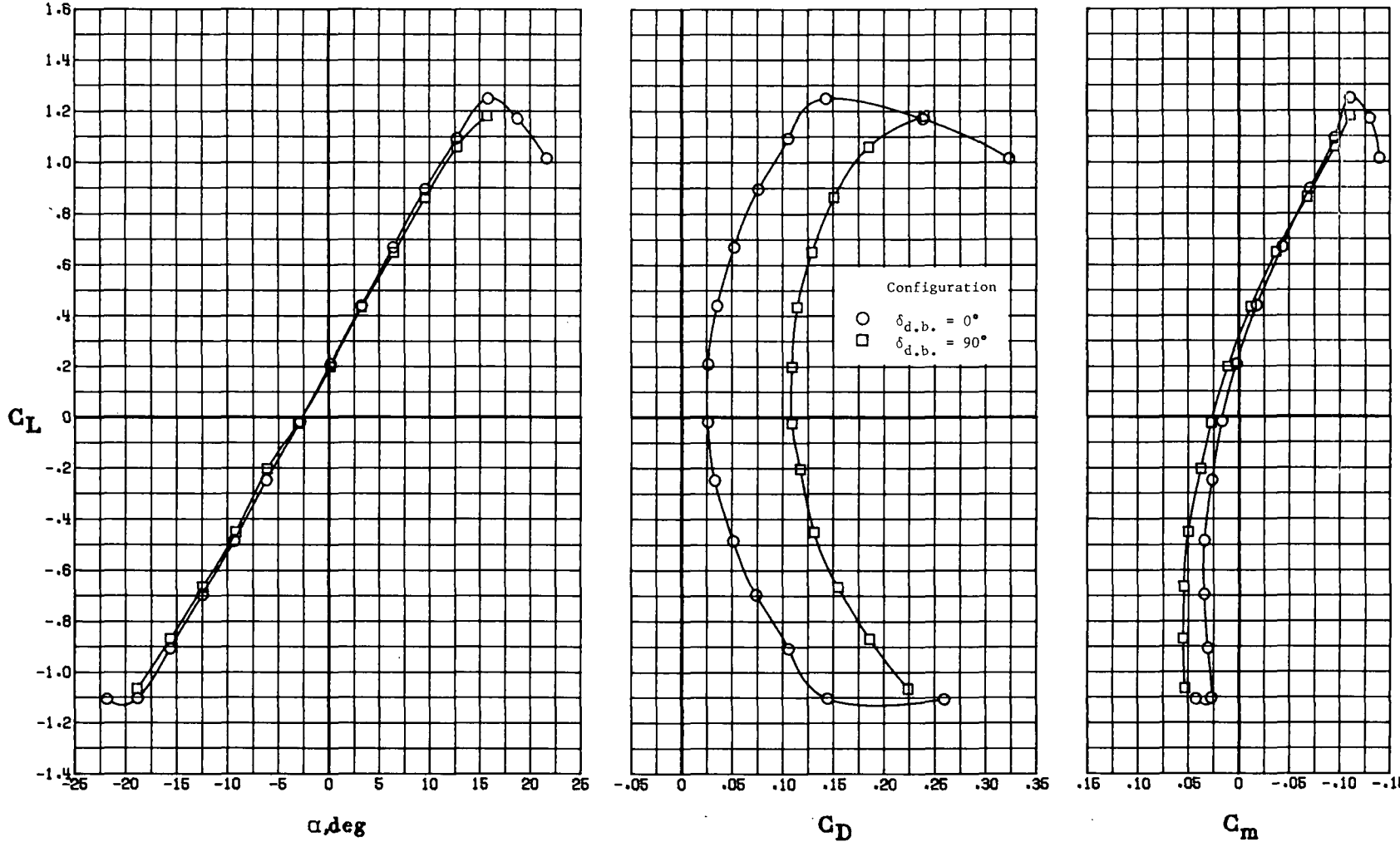

(c) Effect of dive brakes on longitudinal characteristics.

Figure 11.- Continued.

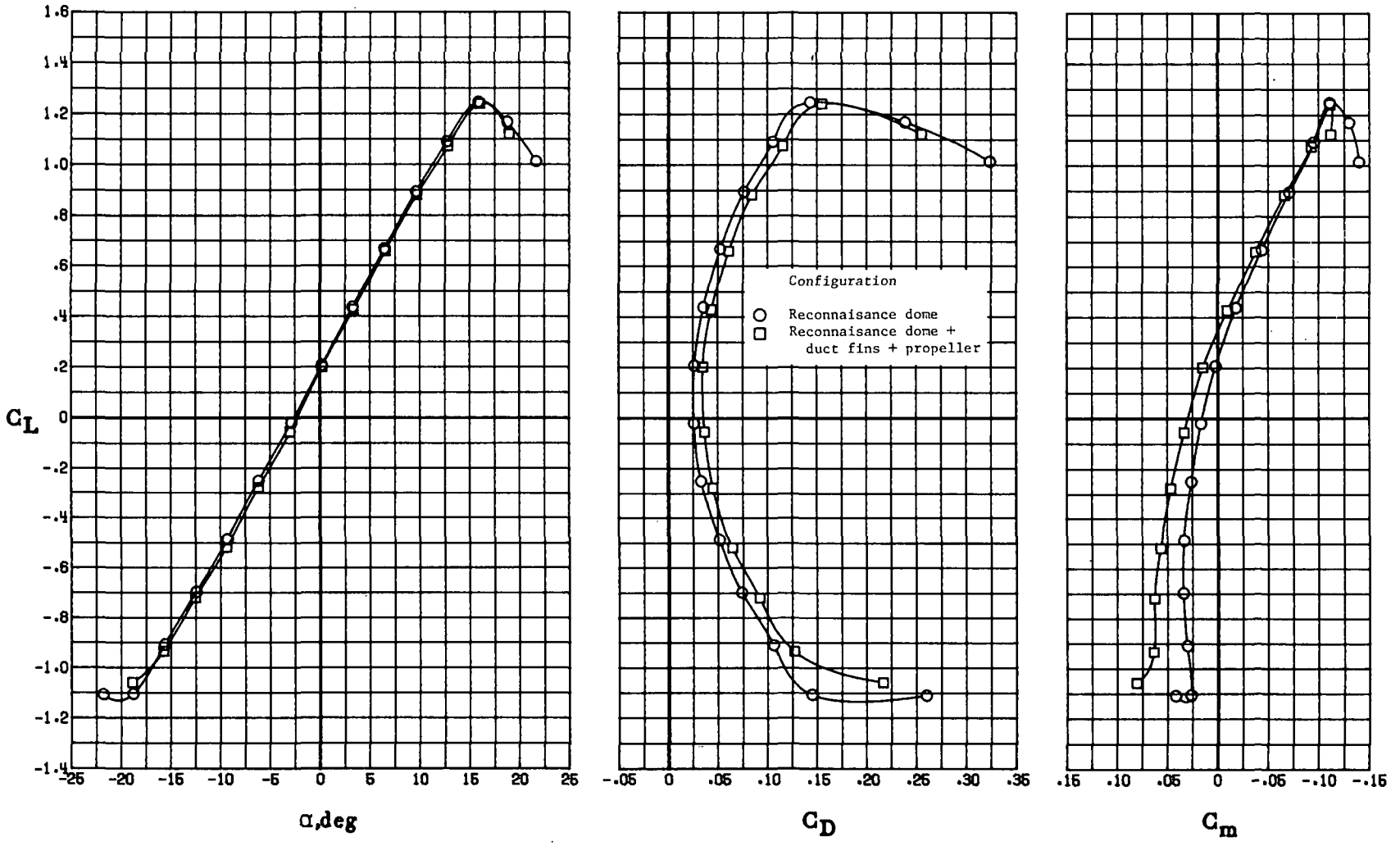

(d) Effect of duct fins on longitudinal characteristics.

Figure 11.- Concluded.

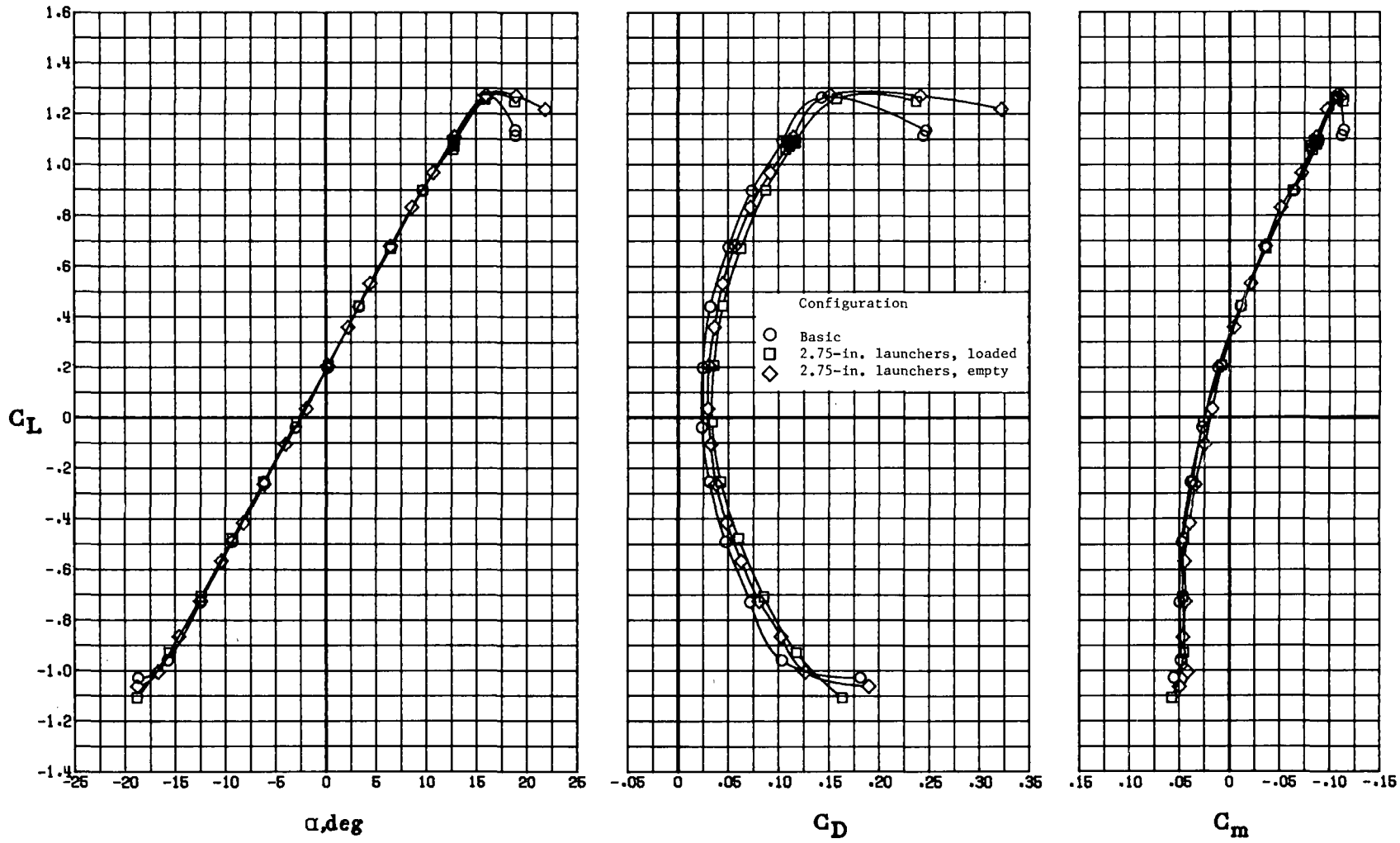

(a) Effect of launchers on overall longitudinal characteristics.

Figure 12.- Longitudinal aerodynamic characteristics of model with 2.75-in. rocket launchers.

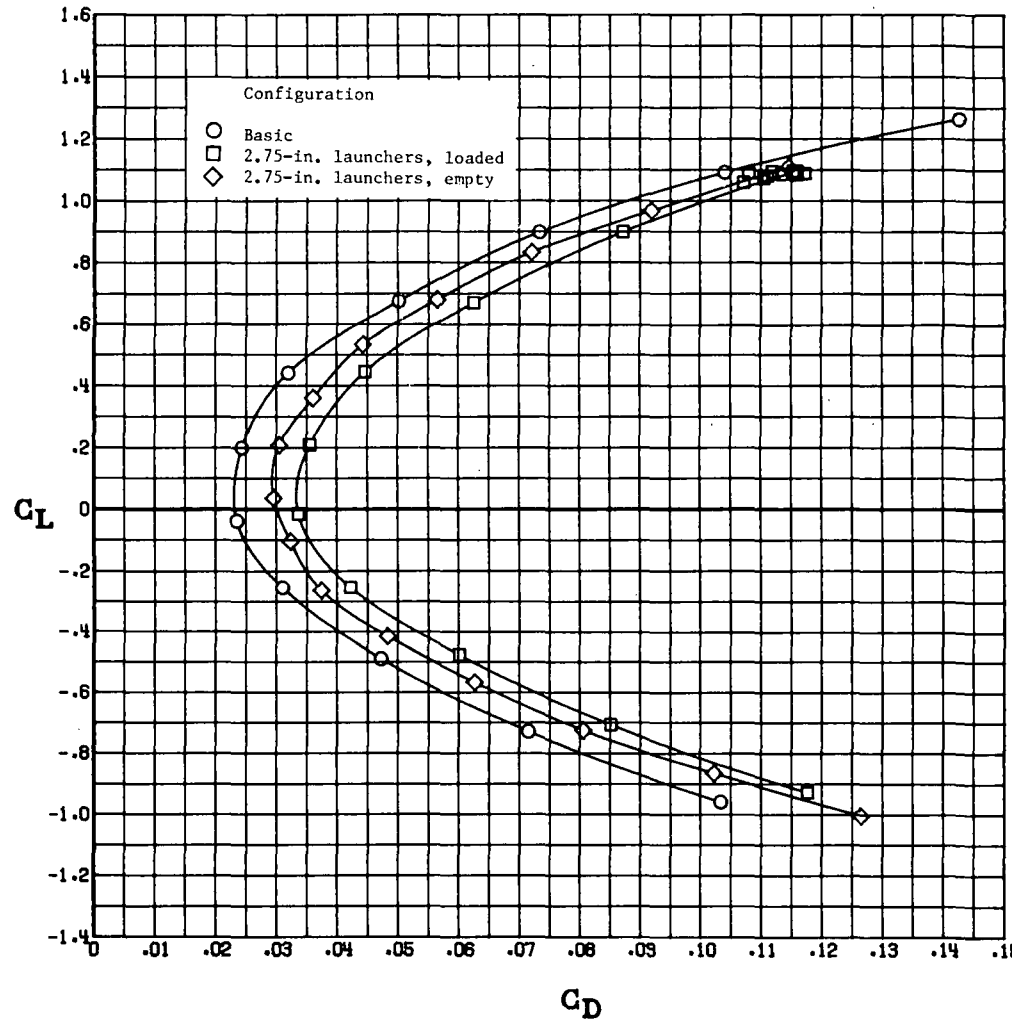

(b) Effect of launchers on drag characteristics.

Figure 12.- Continued.

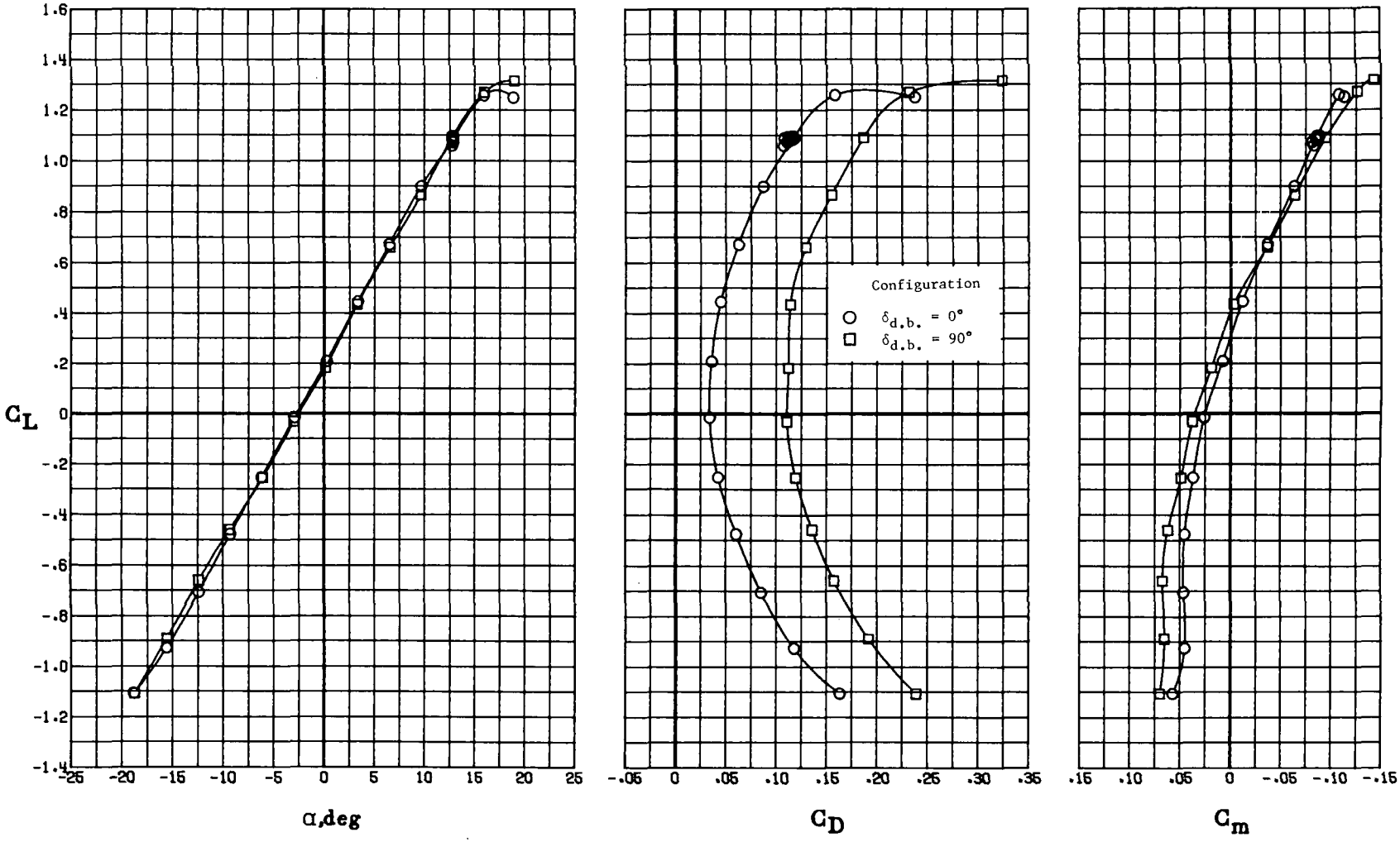

(c) Effect of dive brakes on longitudinal characteristics.

Figure 12.- Continued.

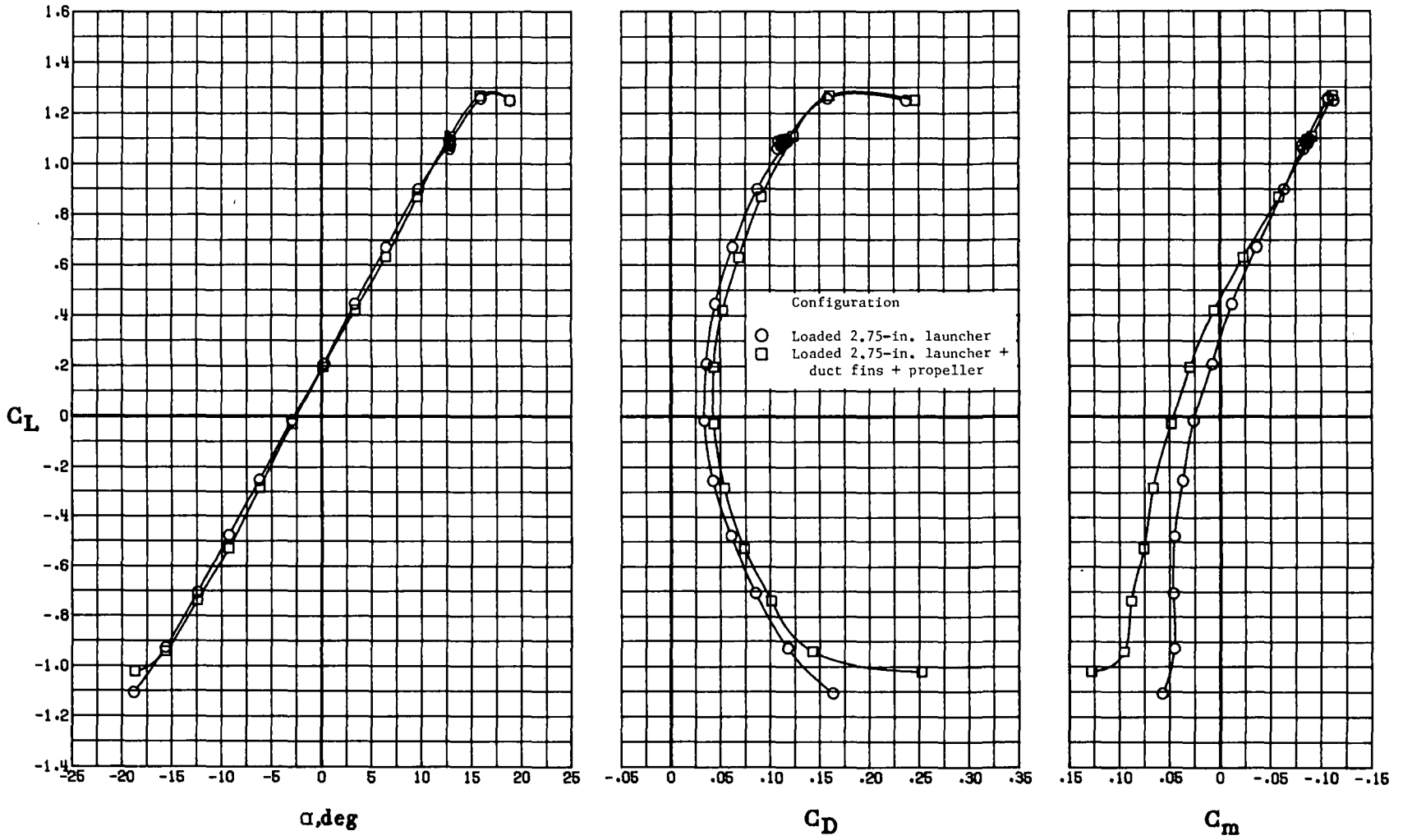

(d) Effect of duct fins on longitudinal characteristics.

Figure 12.- Concluded.

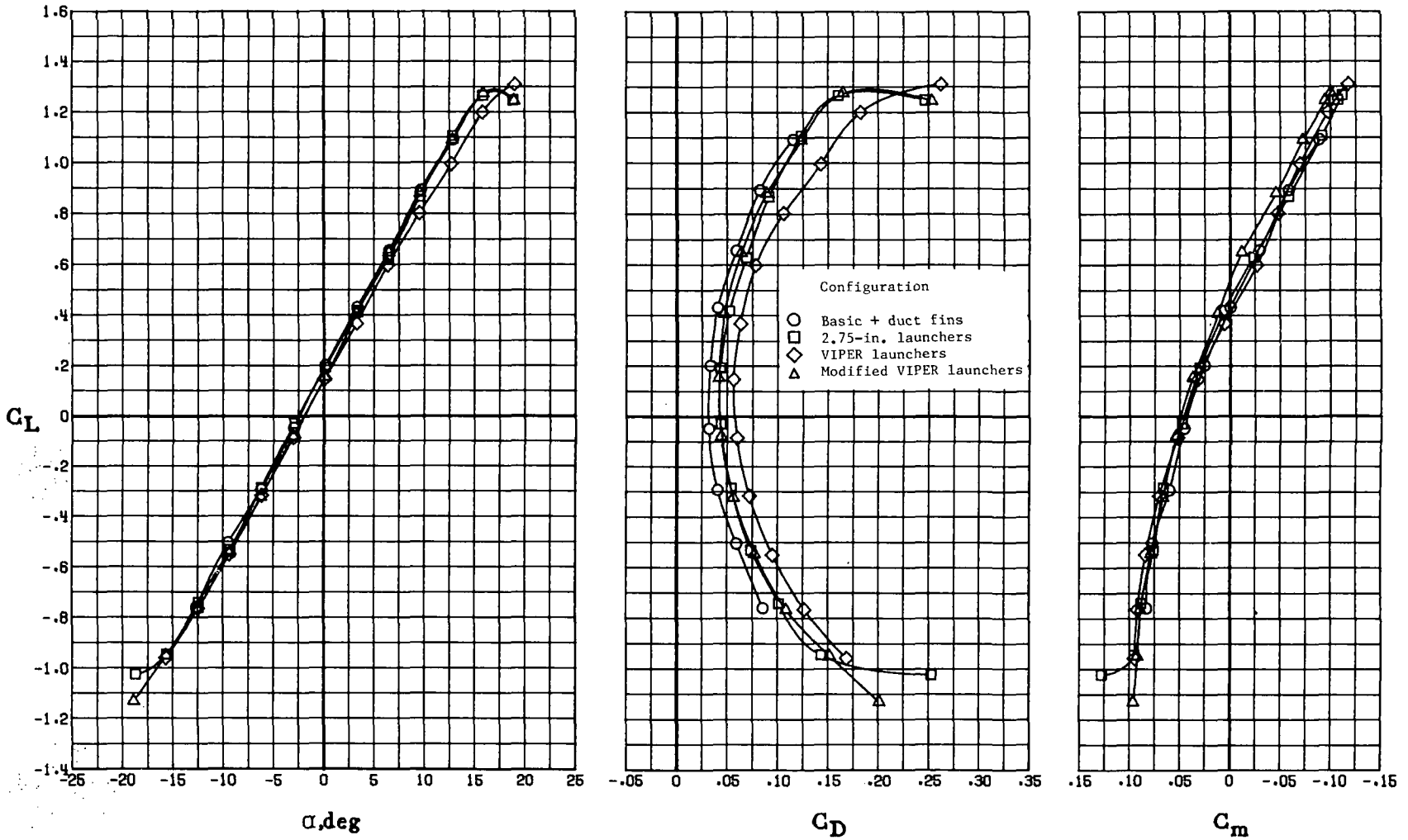

(a) Overall longitudinal characteristics.

Figure 13.- Comparison of longitudinal aerodynamic characteristics of model with and without external stores.

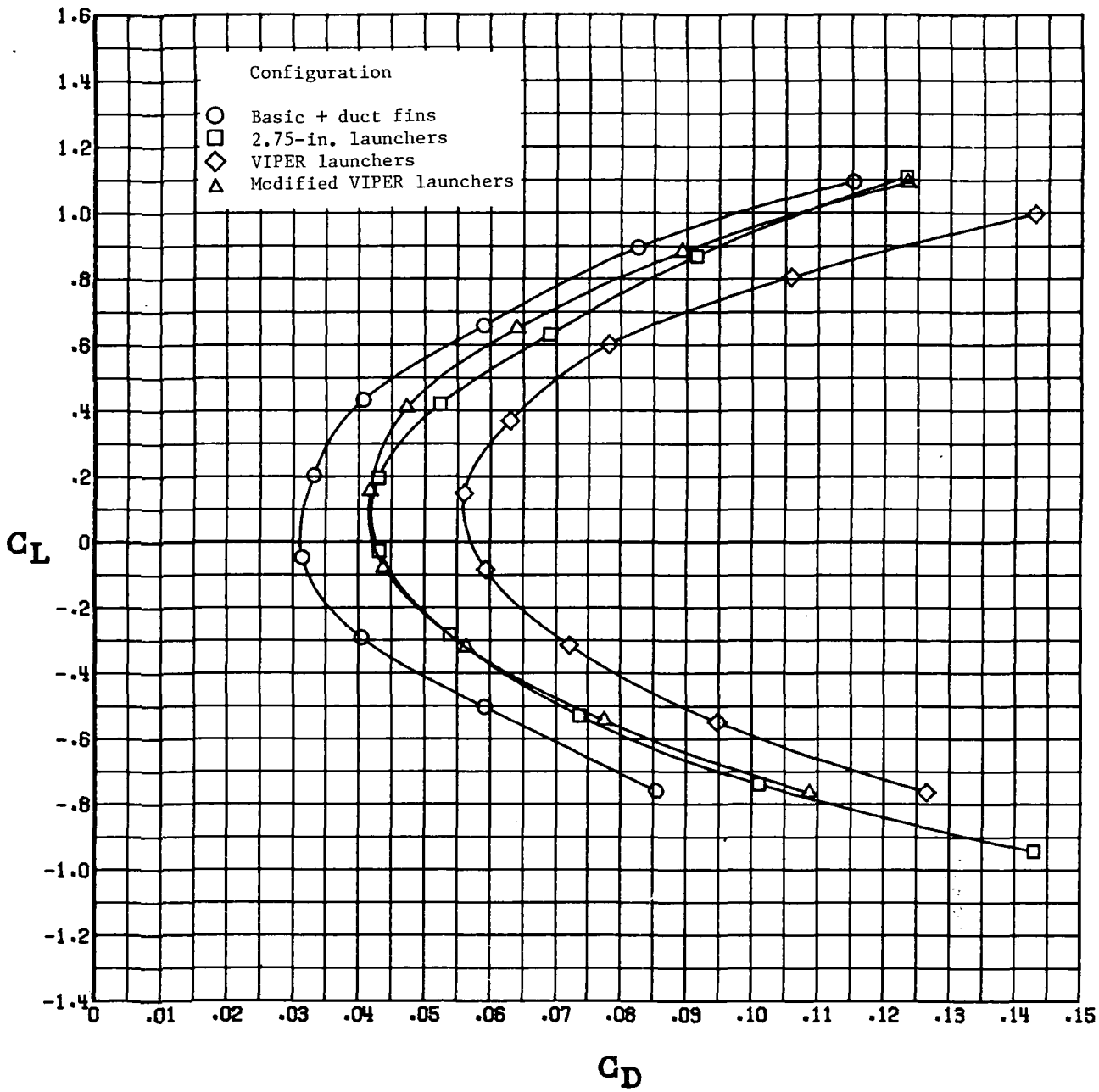

(b) Drag characteristics.

Figure 13.- Concluded.

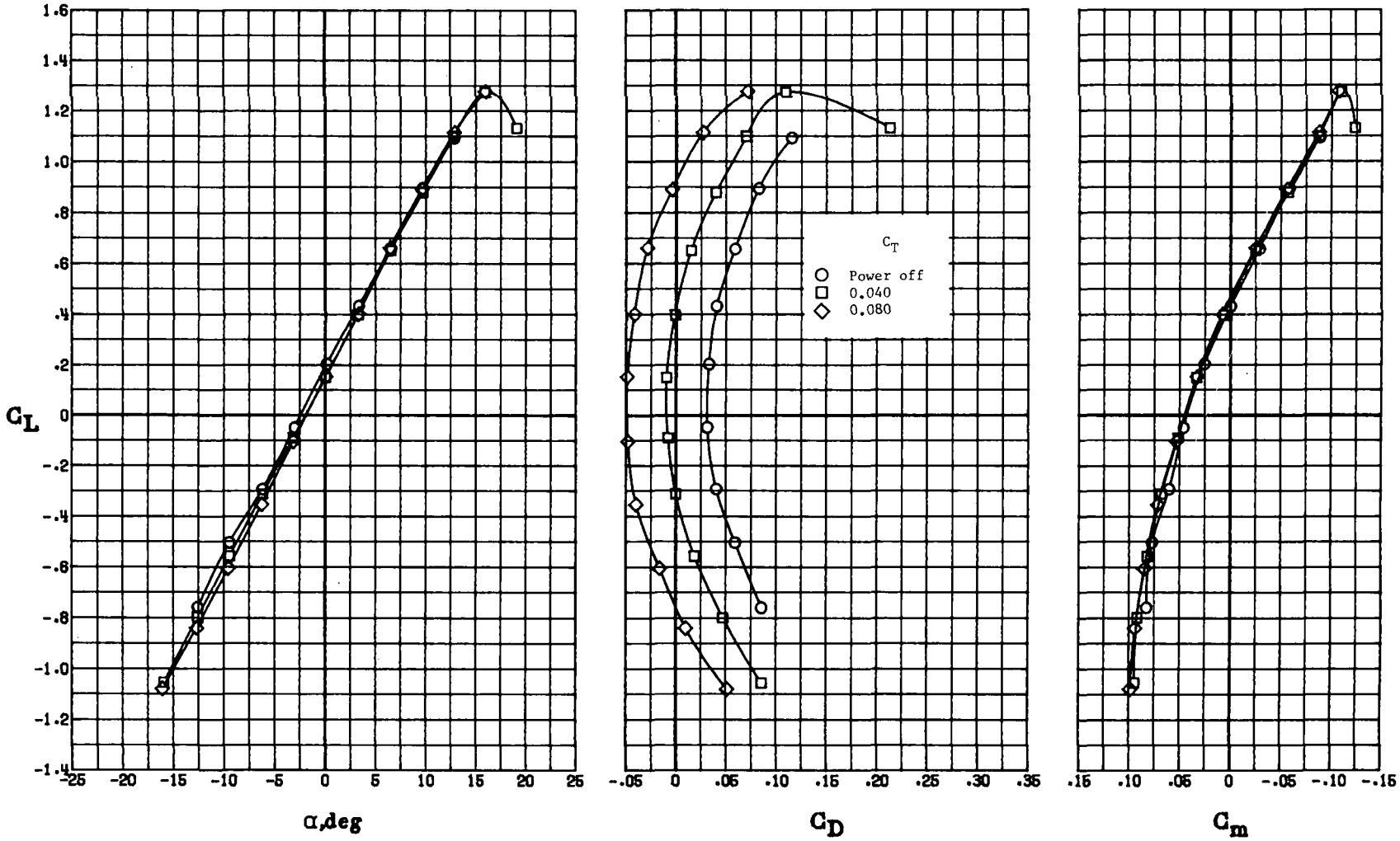

Figure 14.- Effect of power on longitudinal aerodynamic characteristics of model with duct fins.

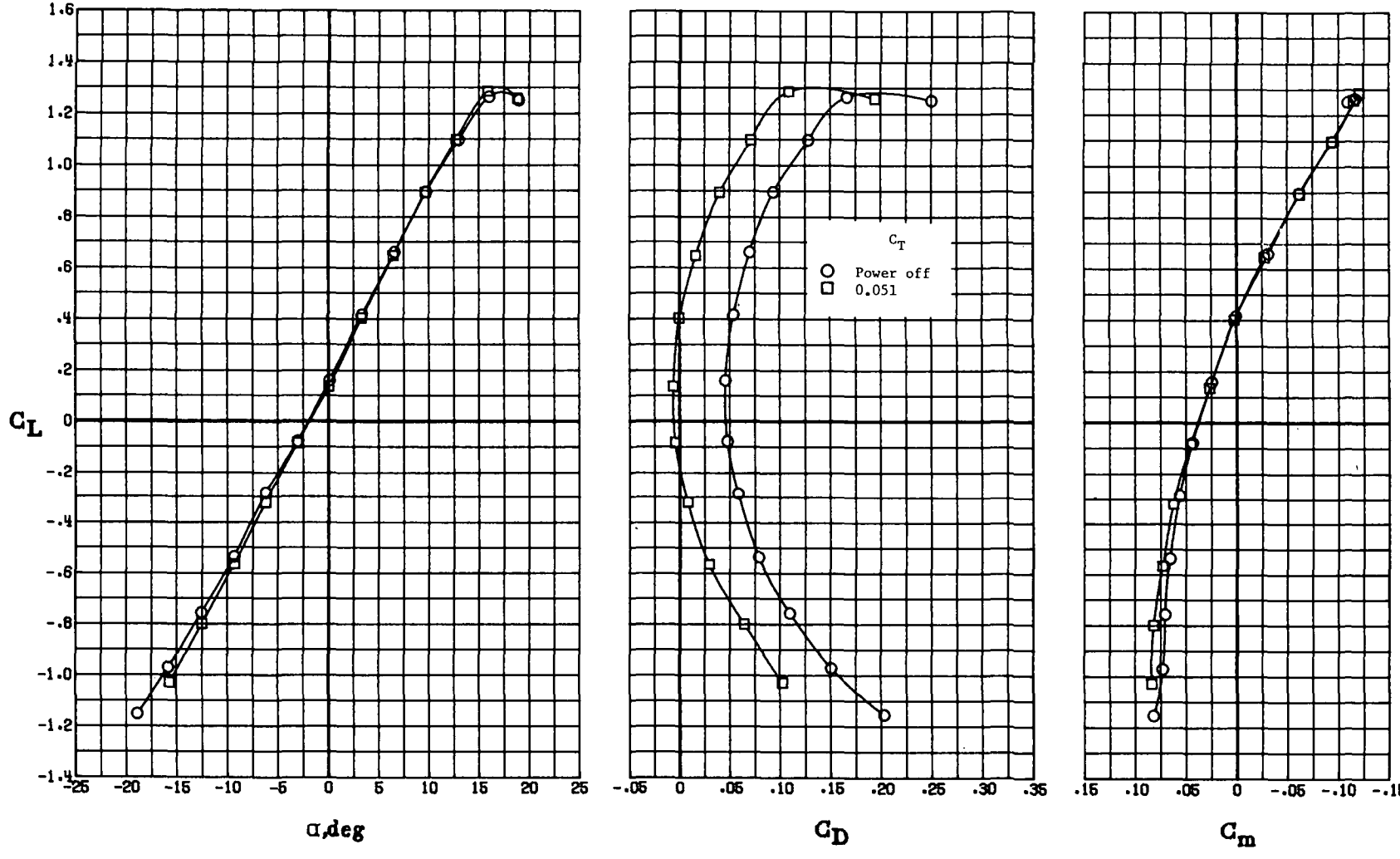

Figure 15.- Effect of power on longitudinal aerodynamic characteristics of fully loaded (reconnaisance dome and 2.75-in. rocket launchers) model with duct fins.

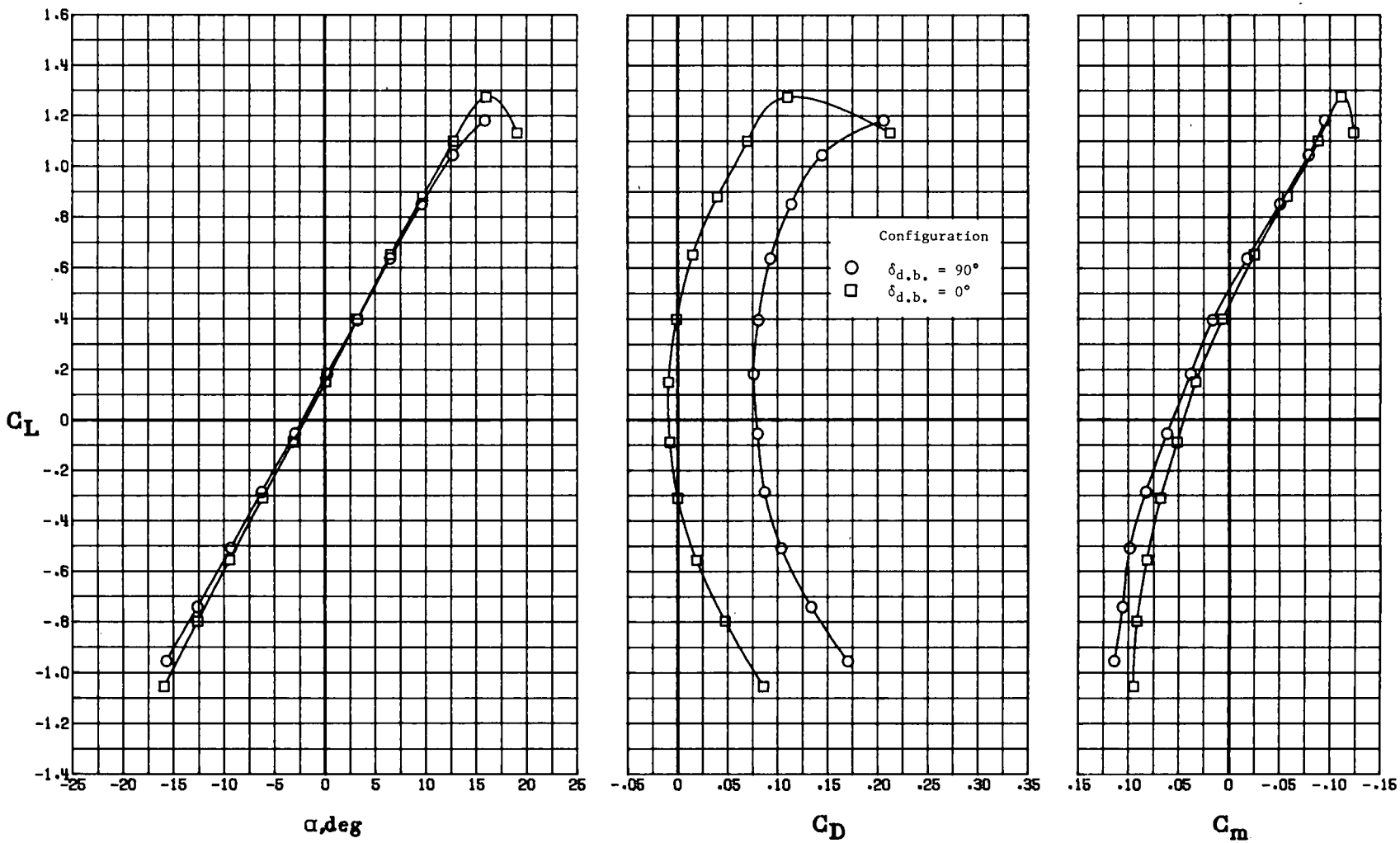

Figure 16.- Effect of dive brakes on longitudinal aerodynamic characteristics of model in basic configuration with duct fins. C_T = 0.040.

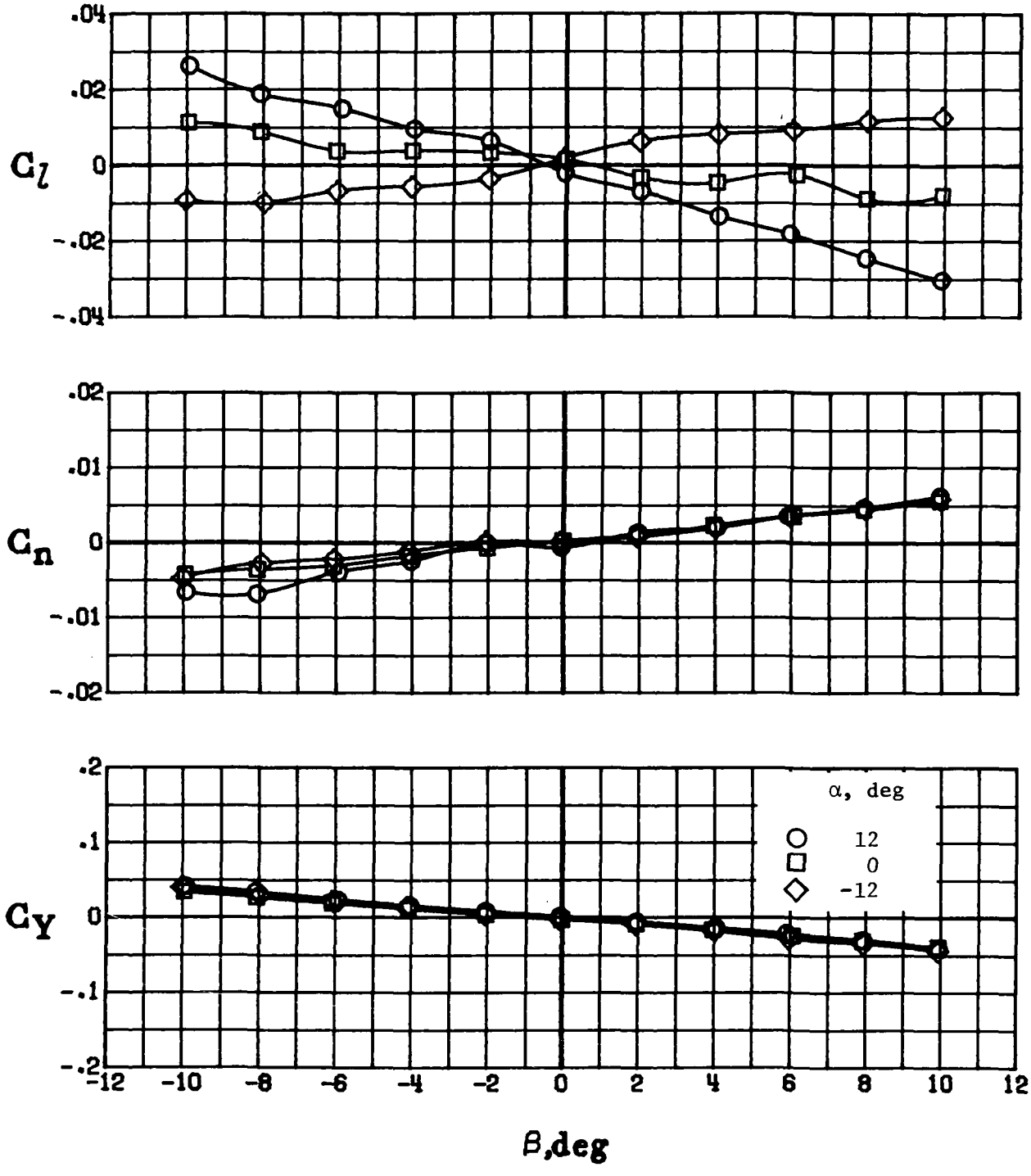

Figure 17.- Lateral-directional aerodynamic characteristics of model in basic configuration.

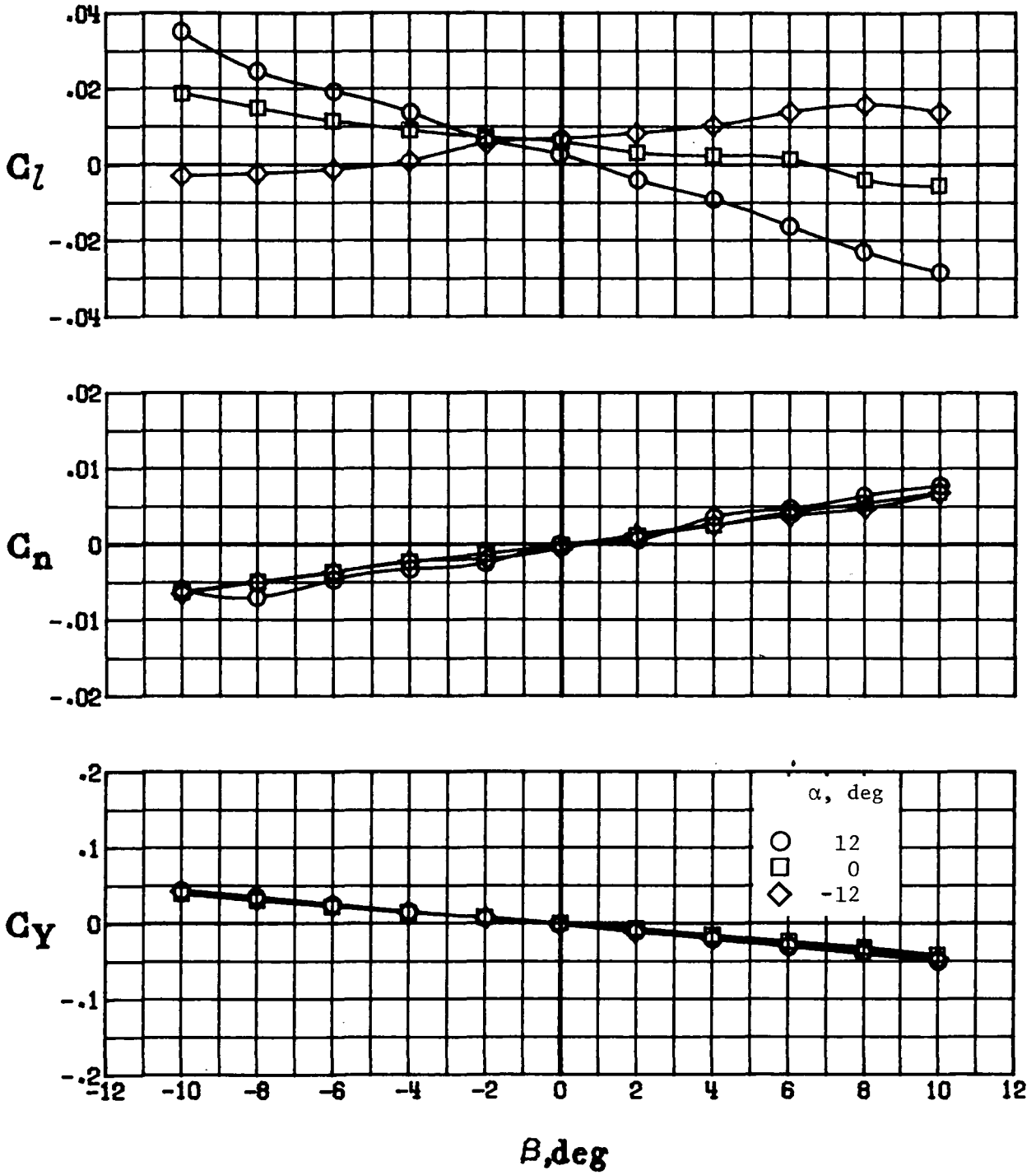

(a) Plain wing tips.

Figure 18.- Lateral-directional aerodynamic characteristics of model with duct fins.

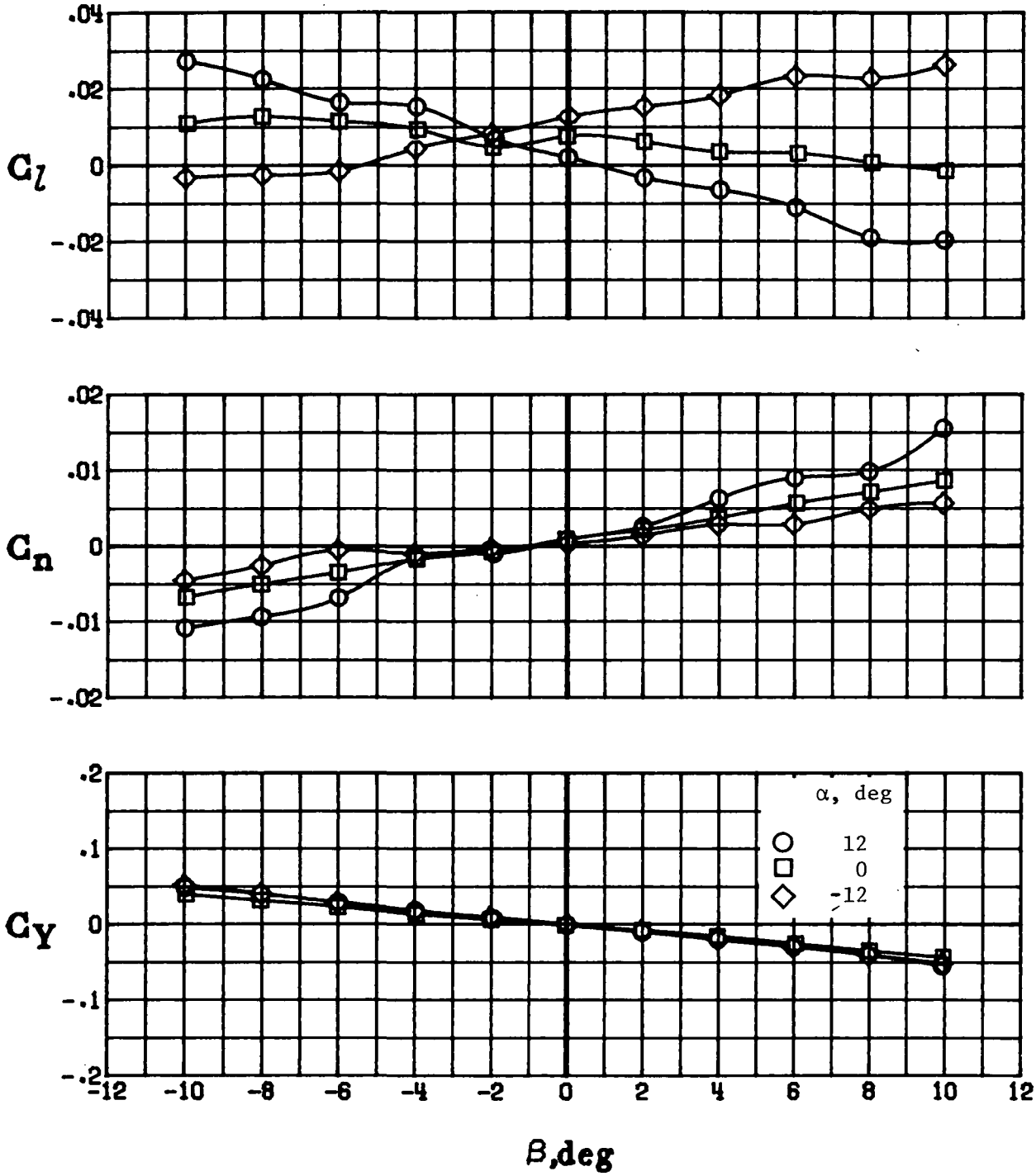

(b) Drooped wing tips.

Figure 18.- Concluded.

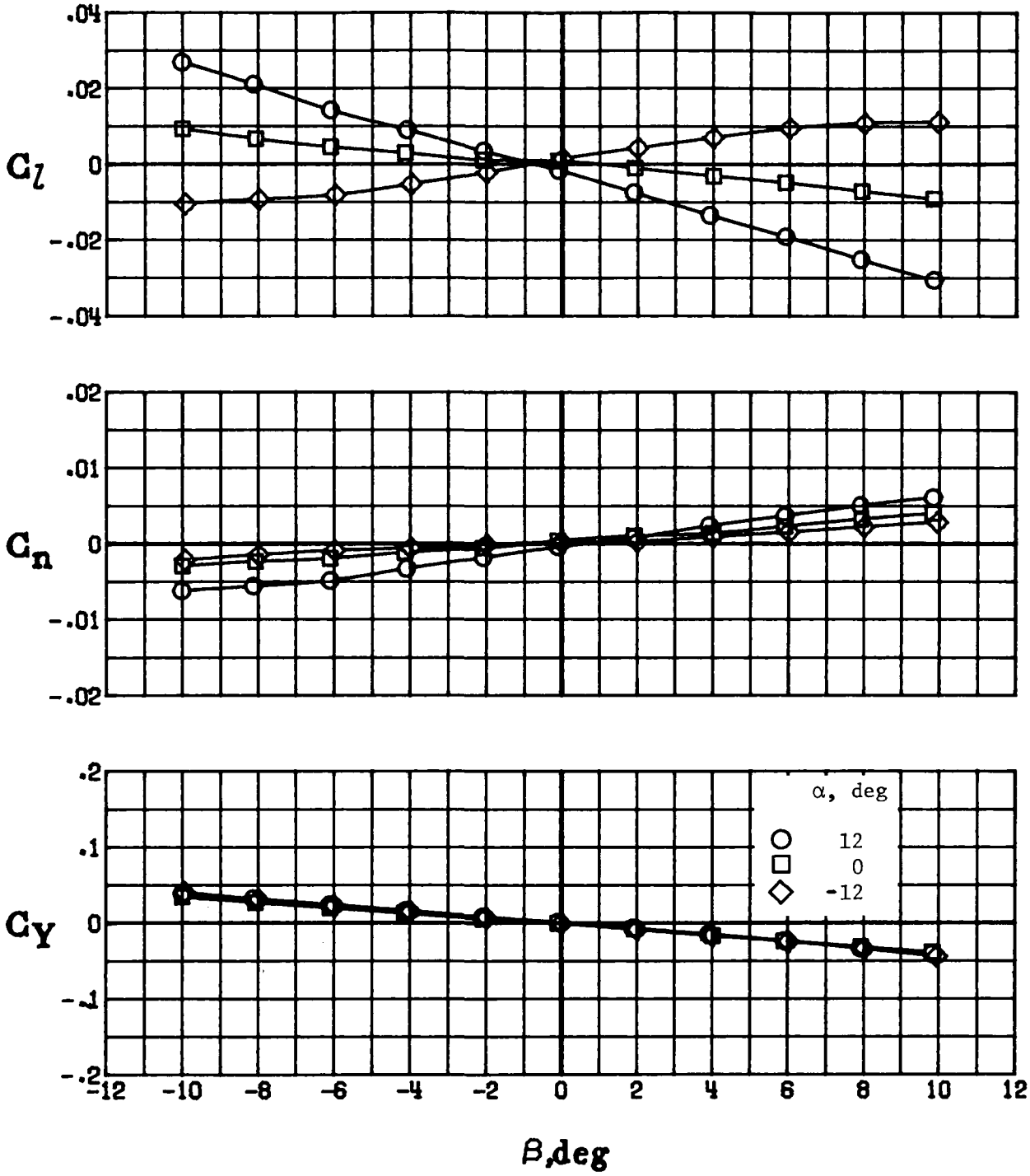

(a) Basic configuration.

Figure 19.- Lateral-directional aerodynamic characteristics of model with reconnaisance dome.

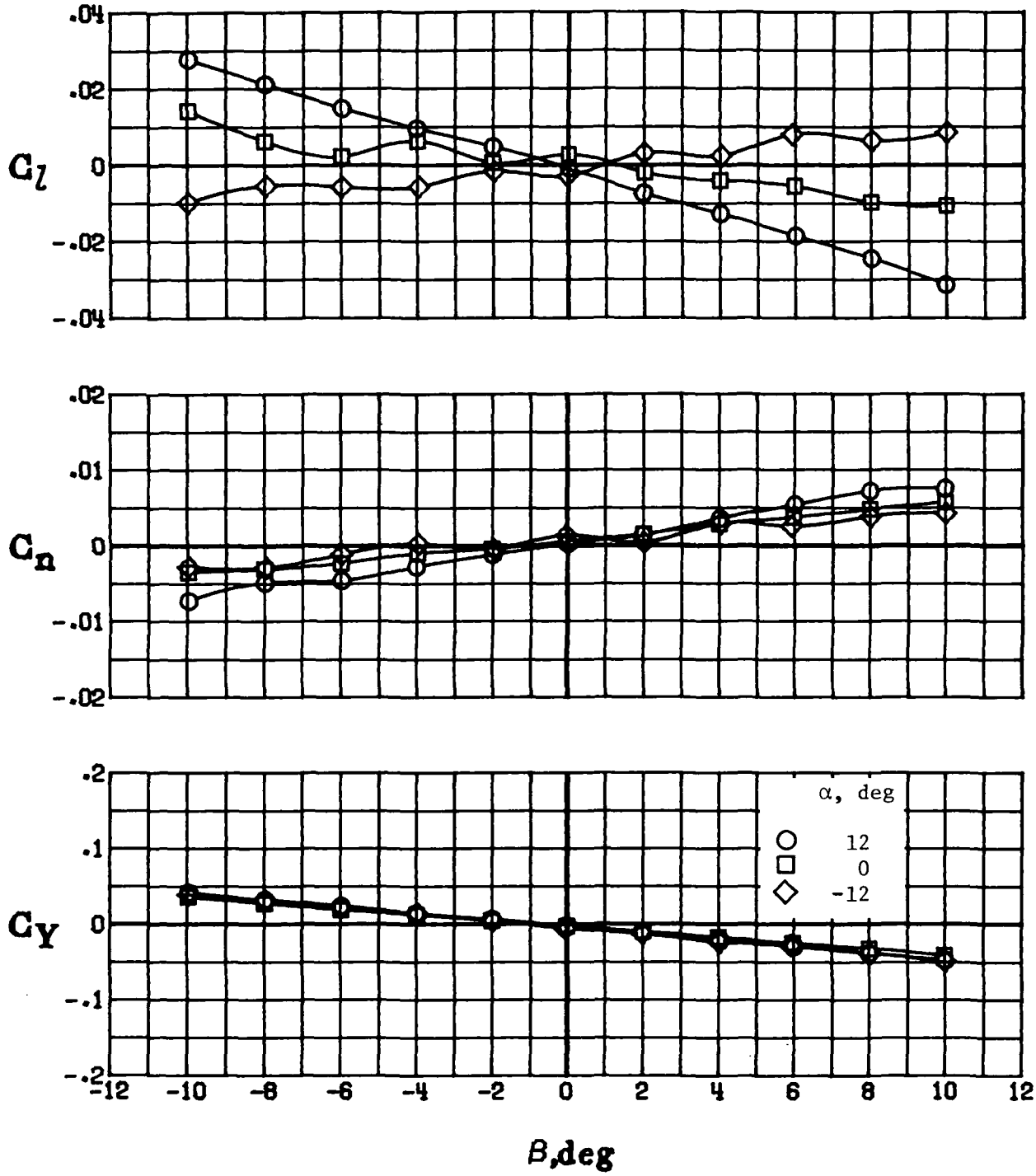

(b) Basic configuration and duct fins.

Figure 19.- Concluded.

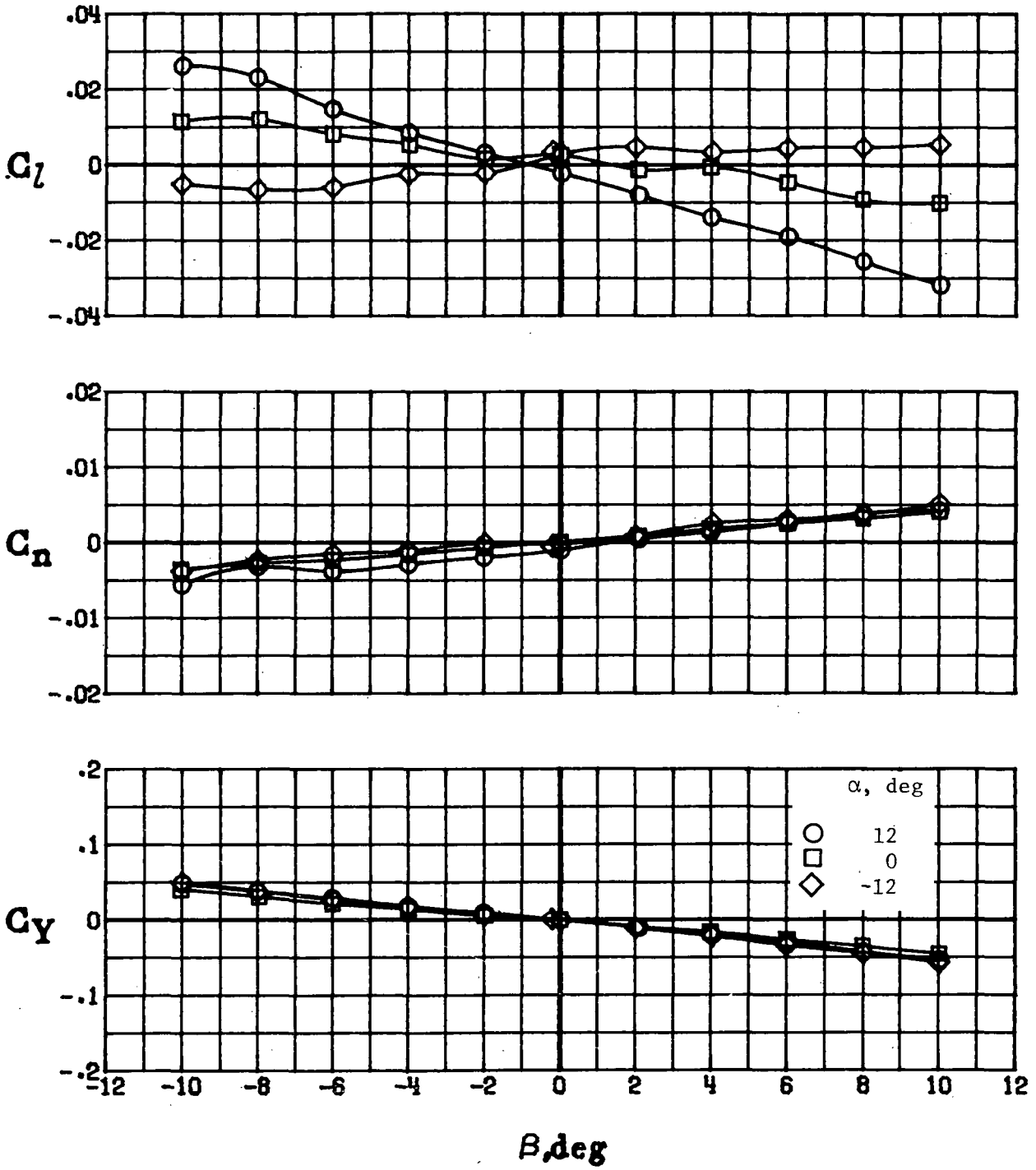

(a) Basic configuration.

Figure 20.- Lateral-directional aerodynamic characteristics of model with 2.75-in. rocket launchers.

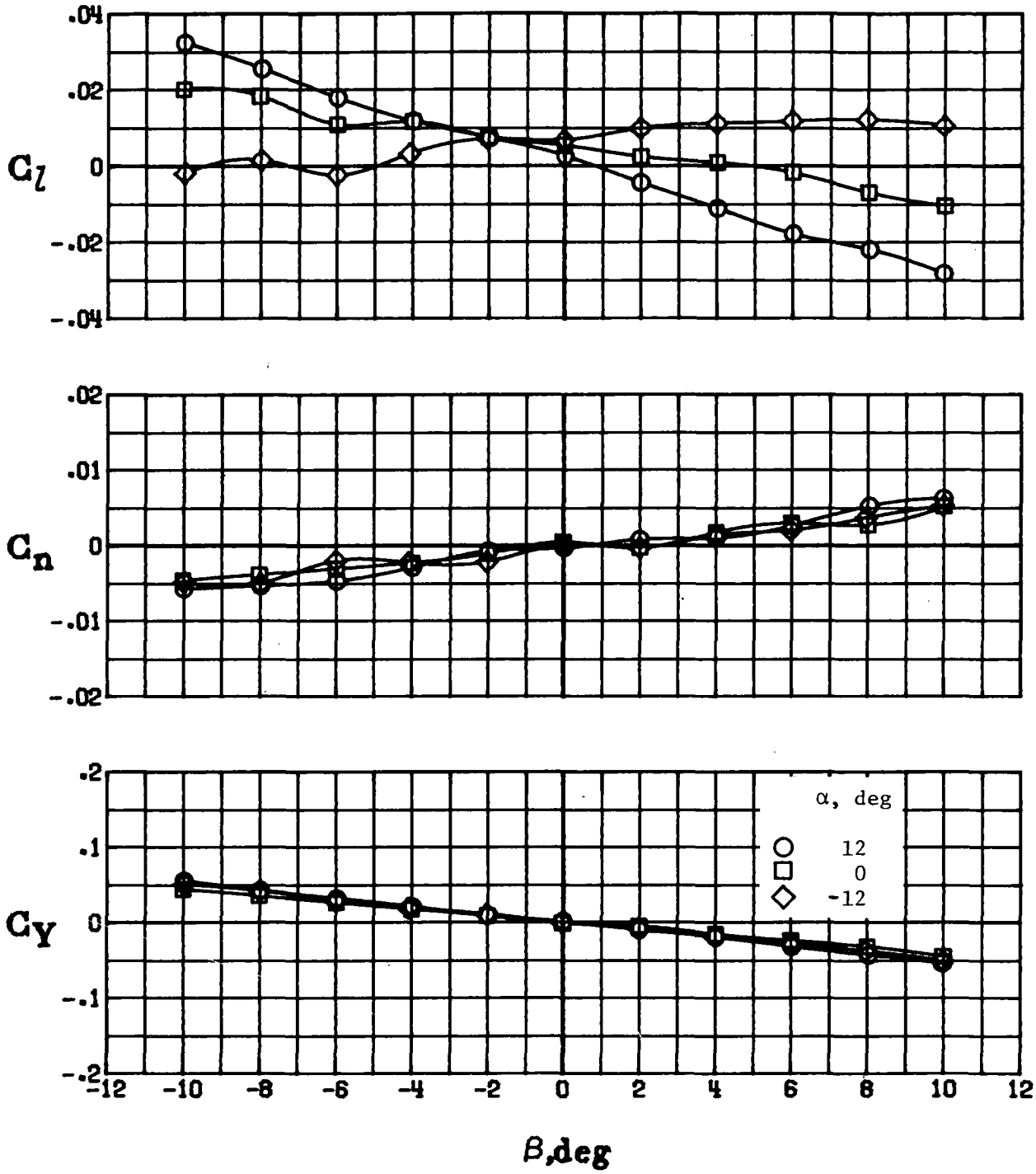

(b) Basic configuration and duct fins.

Figure 20.- Concluded.

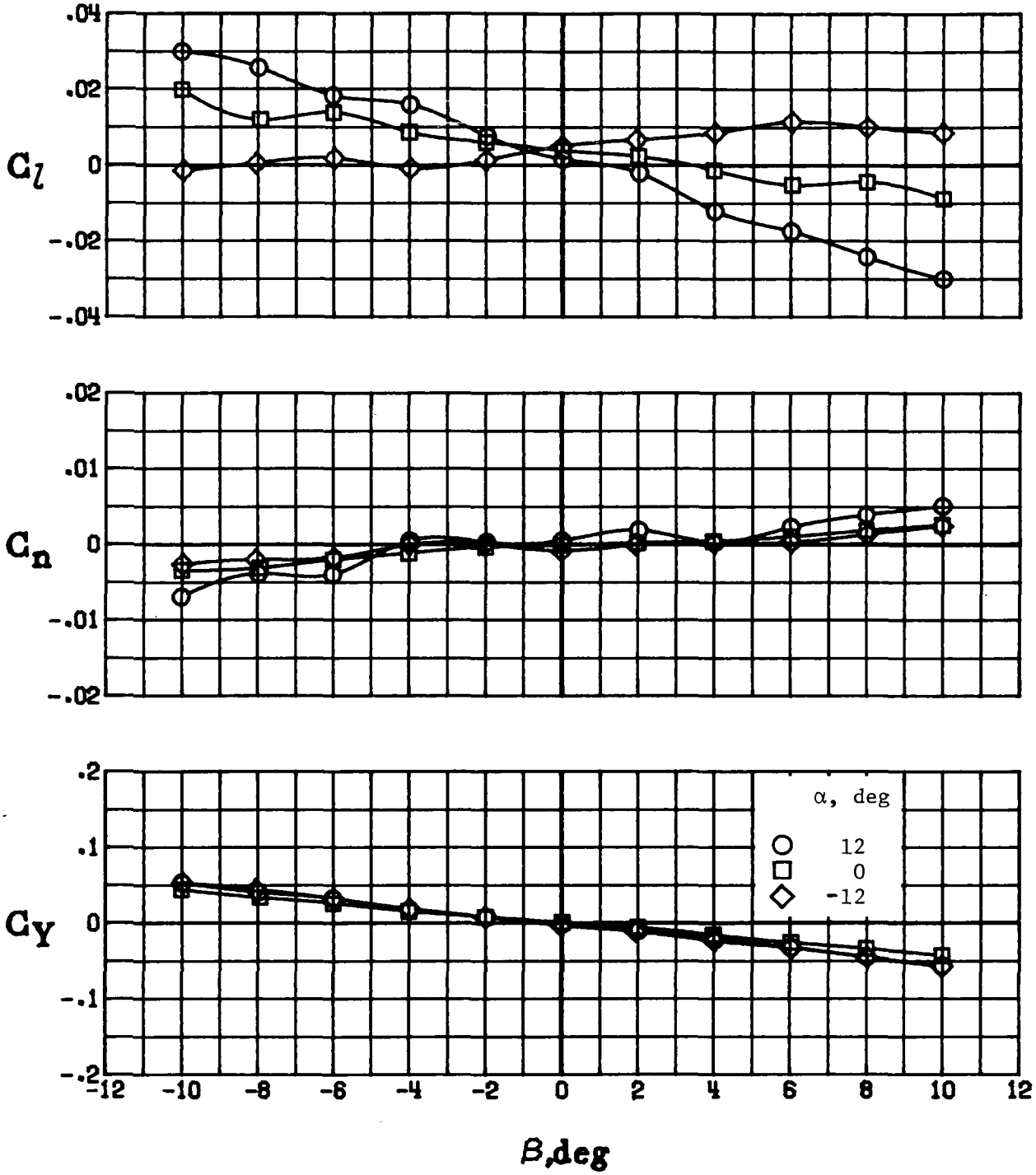

(a) Launcher fins off.

Figure 21.- Effect of launcher fins on lateral-directional aerodynamic characteristics of fully loaded (reconnaisance dome and 2.75-in. rocket launcher) model with duct fins.

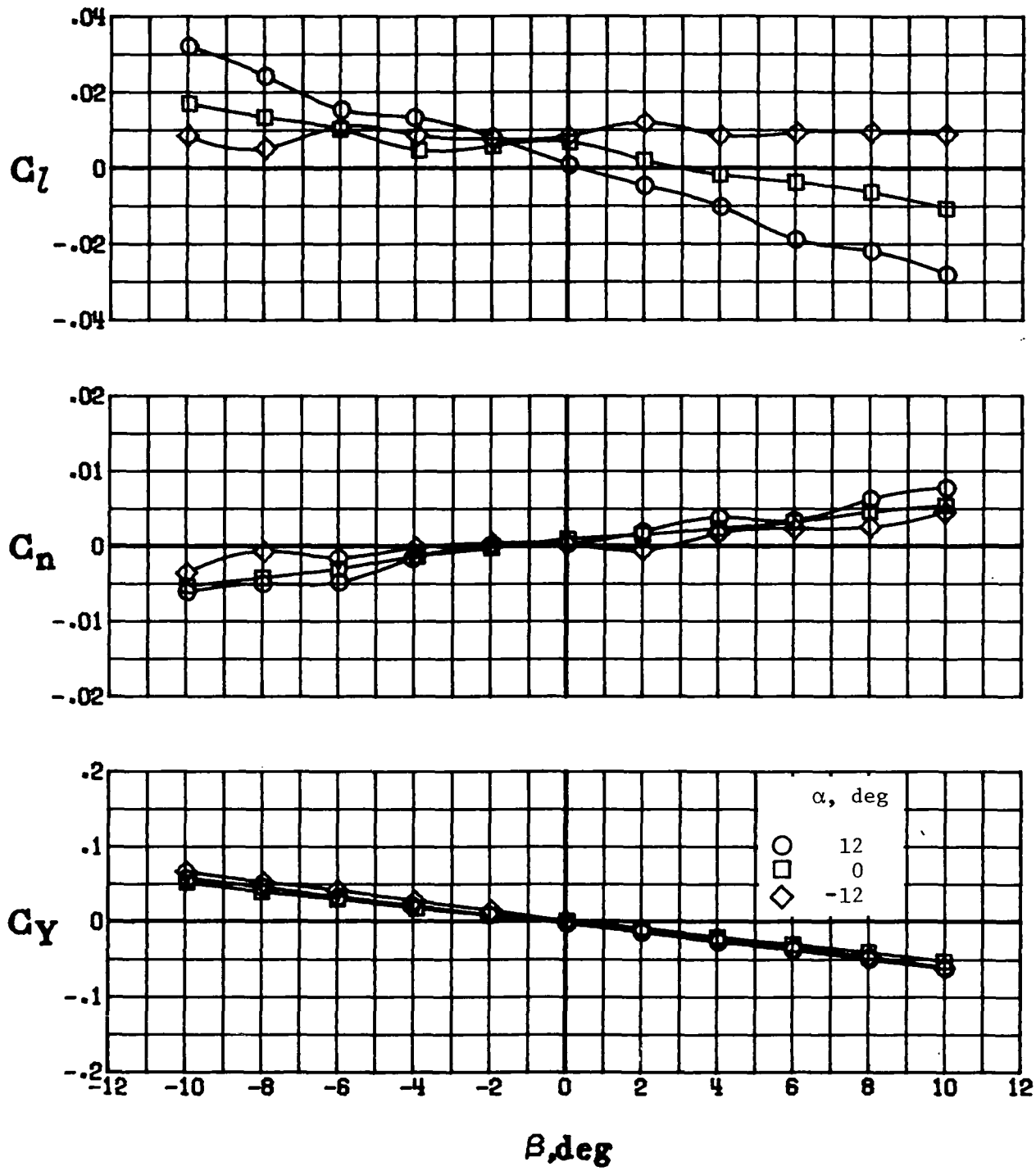

(b) Launcher fins on.

Figure 21.- Concluded.

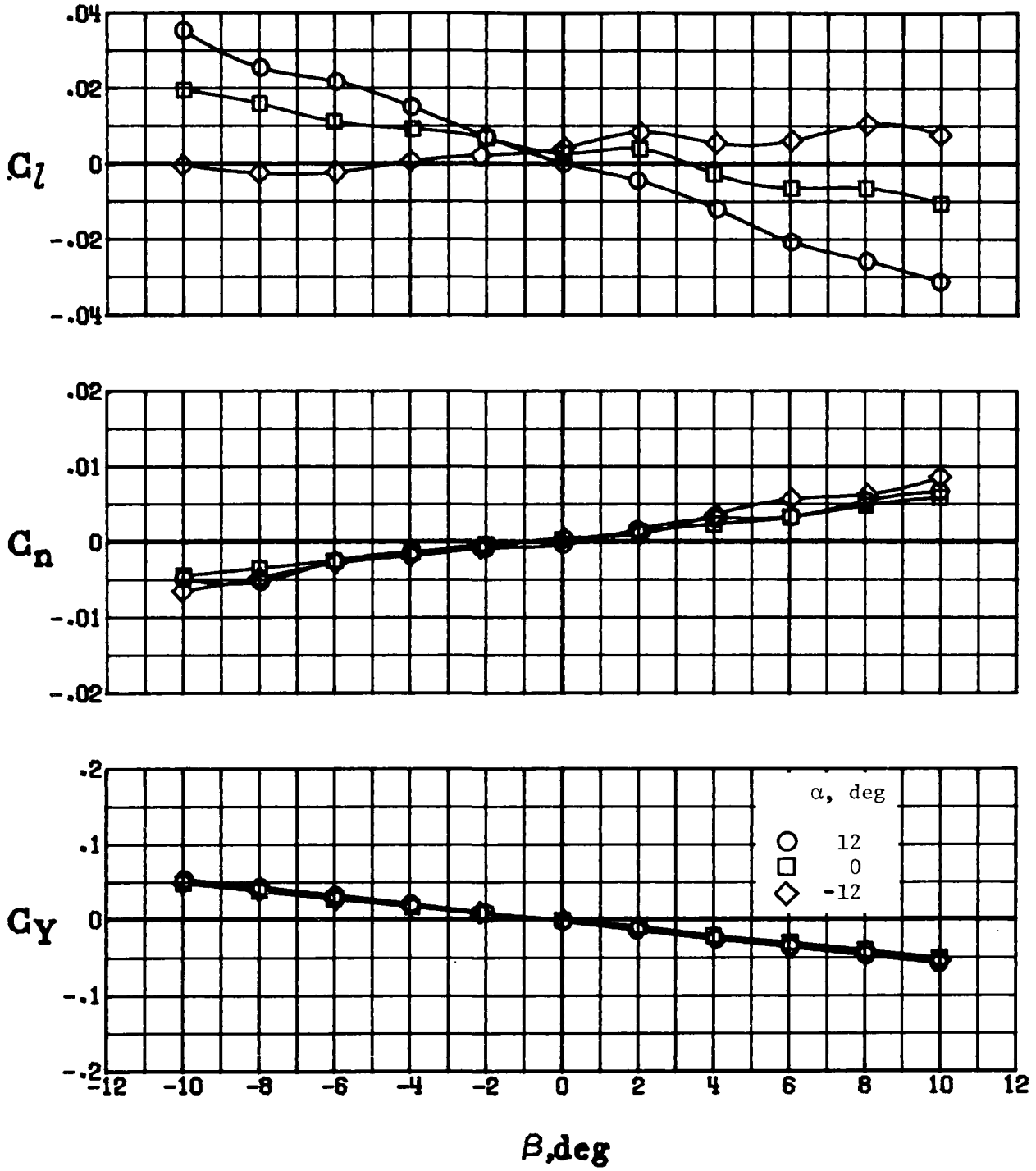

Figure 22.- Lateral-directional aerodynamic characteristics of model with VIPER launcher. Duct fins on.

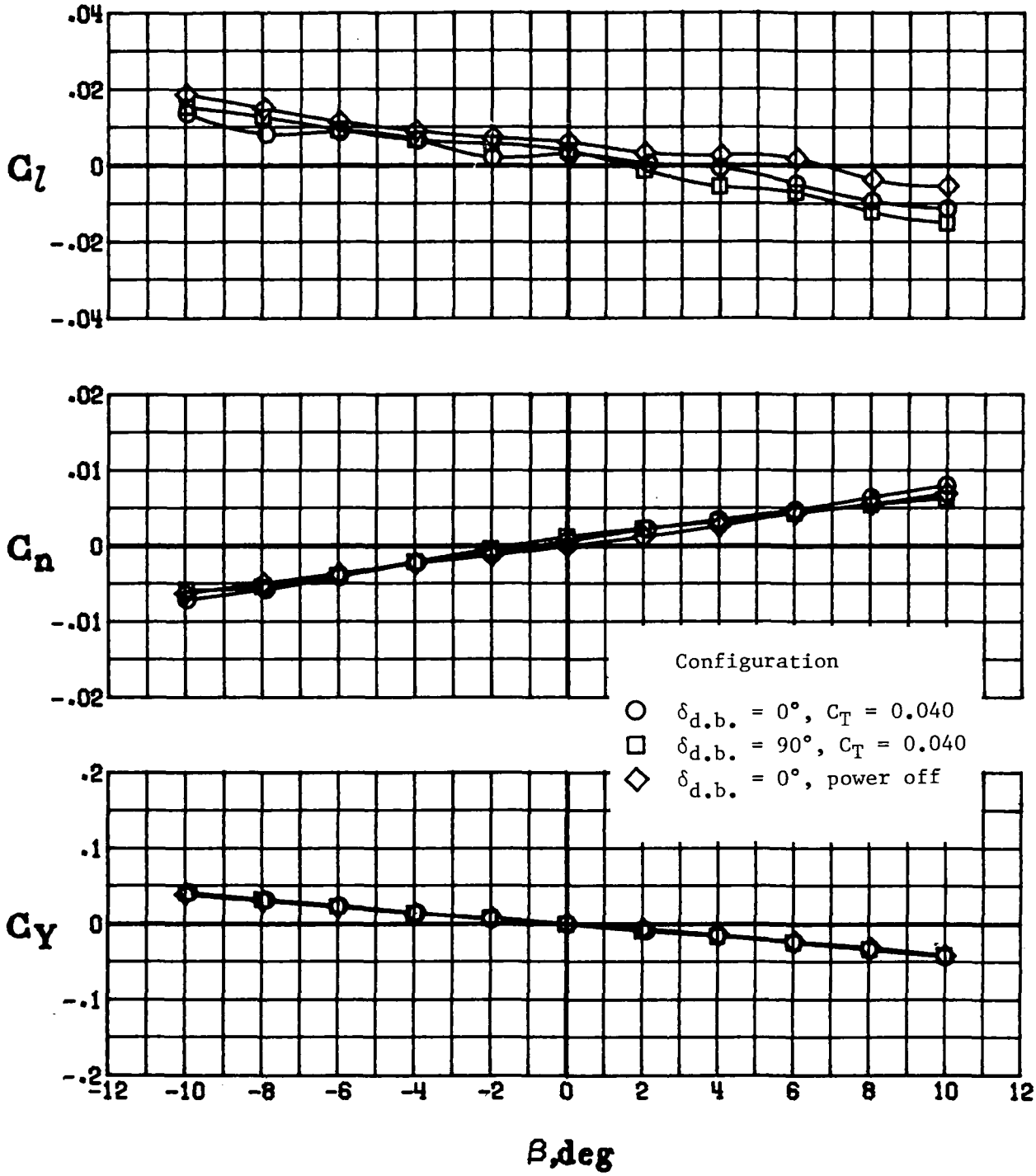

Figure 23.- Effect of power and dive brakes on lateral-directional aerodynamic characteristics of model. Duct fins on.

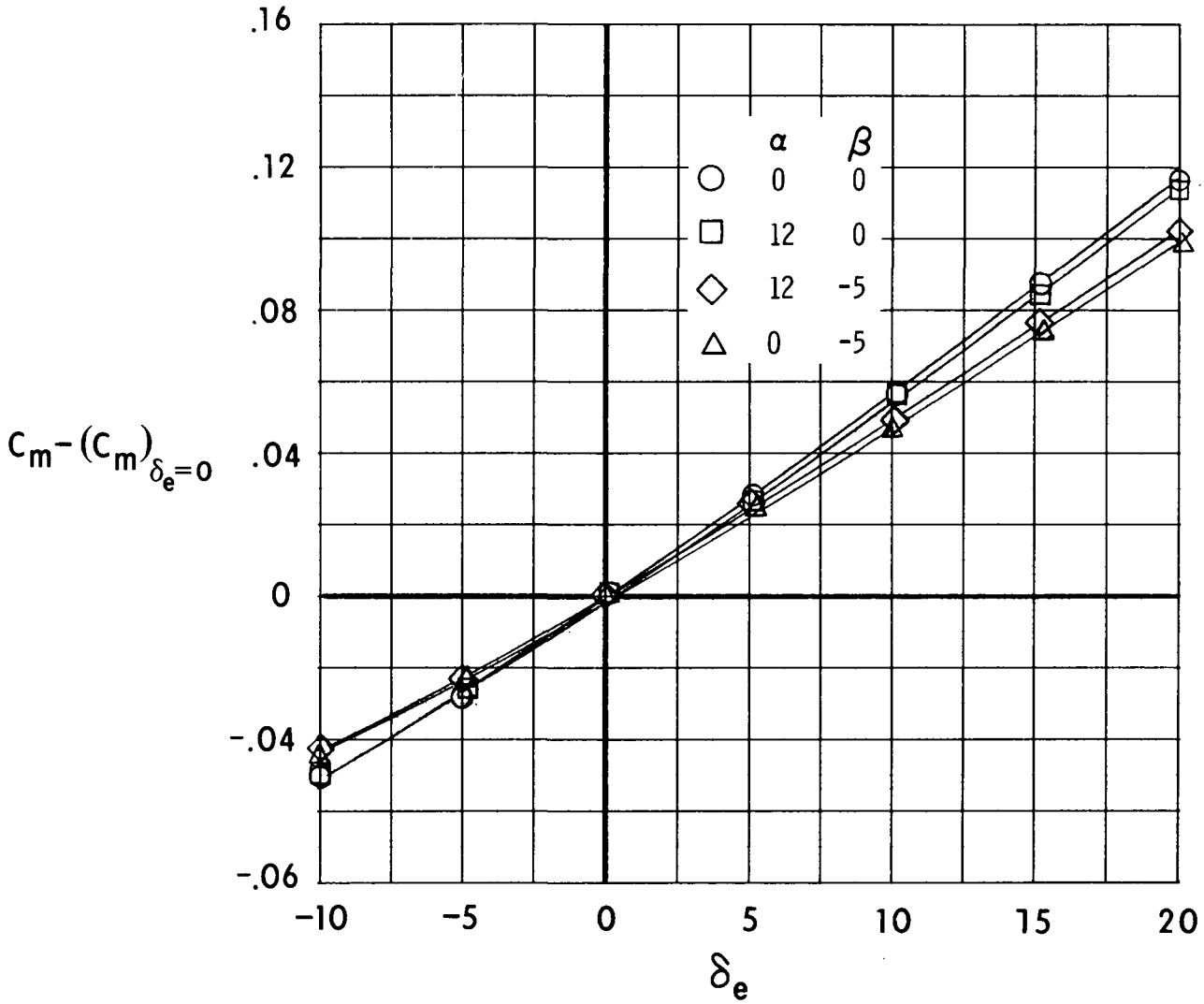

(a) $\delta_{d.b.} = 0^o$.

Figure 24.- Effect of elevator deflection on pitching-moment characteristics of model. Duct fins on.

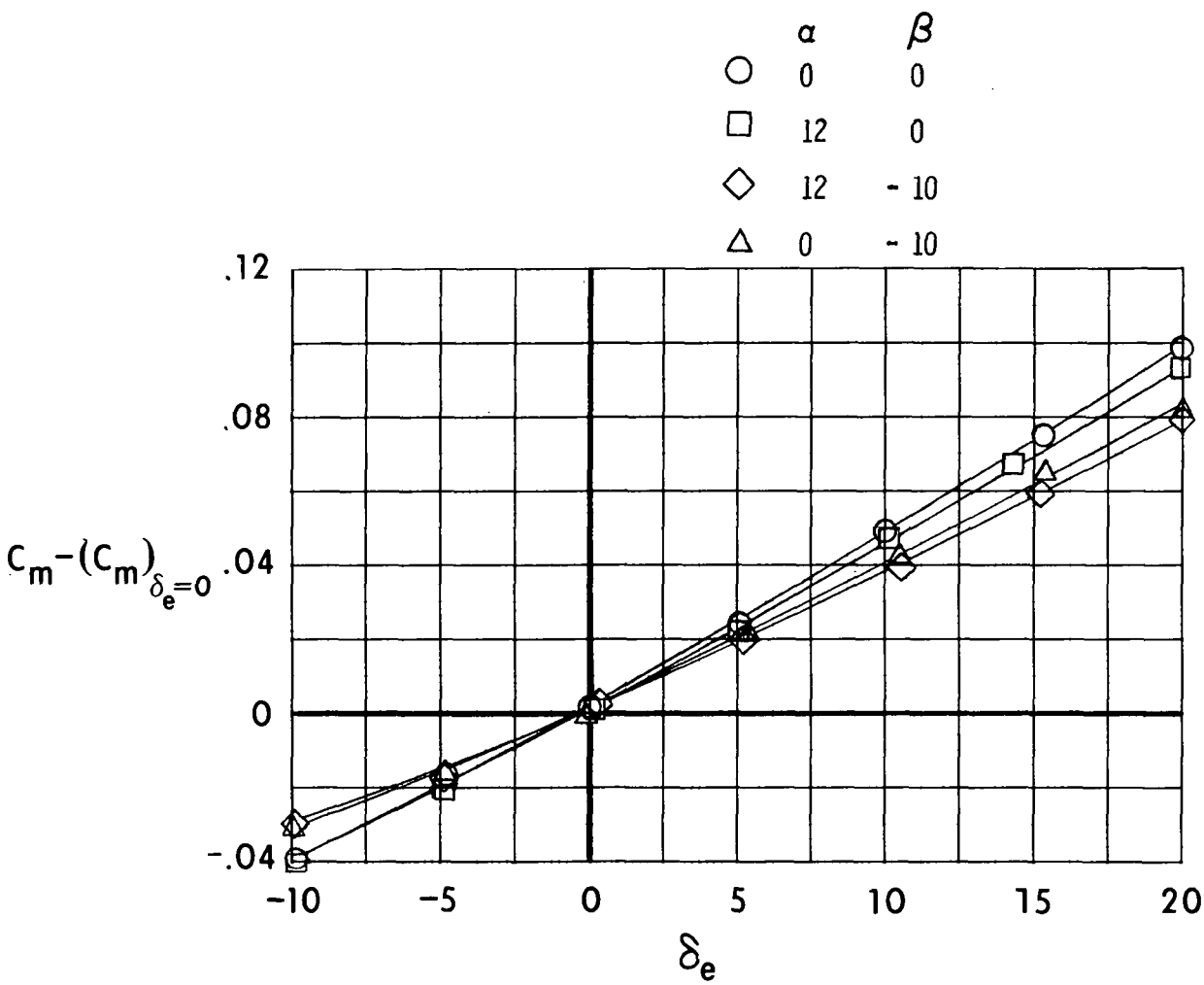

(b) $\delta_{d.b.} = 90^{o}$.

Figure 24.- Concluded.

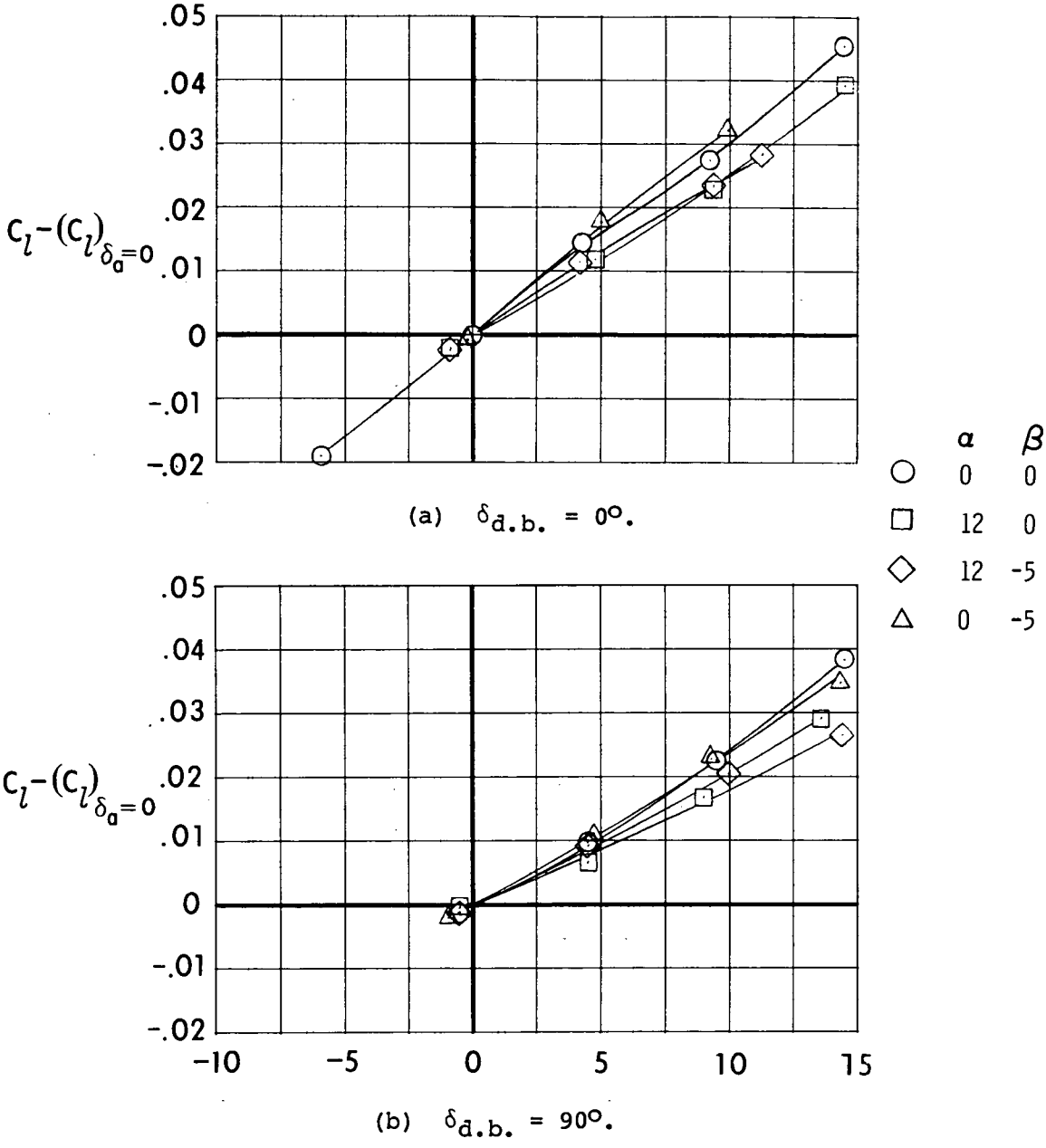

Figure 25.- Effect of aileron deflection on rolling-moment characteristics of model. Duct fins on.

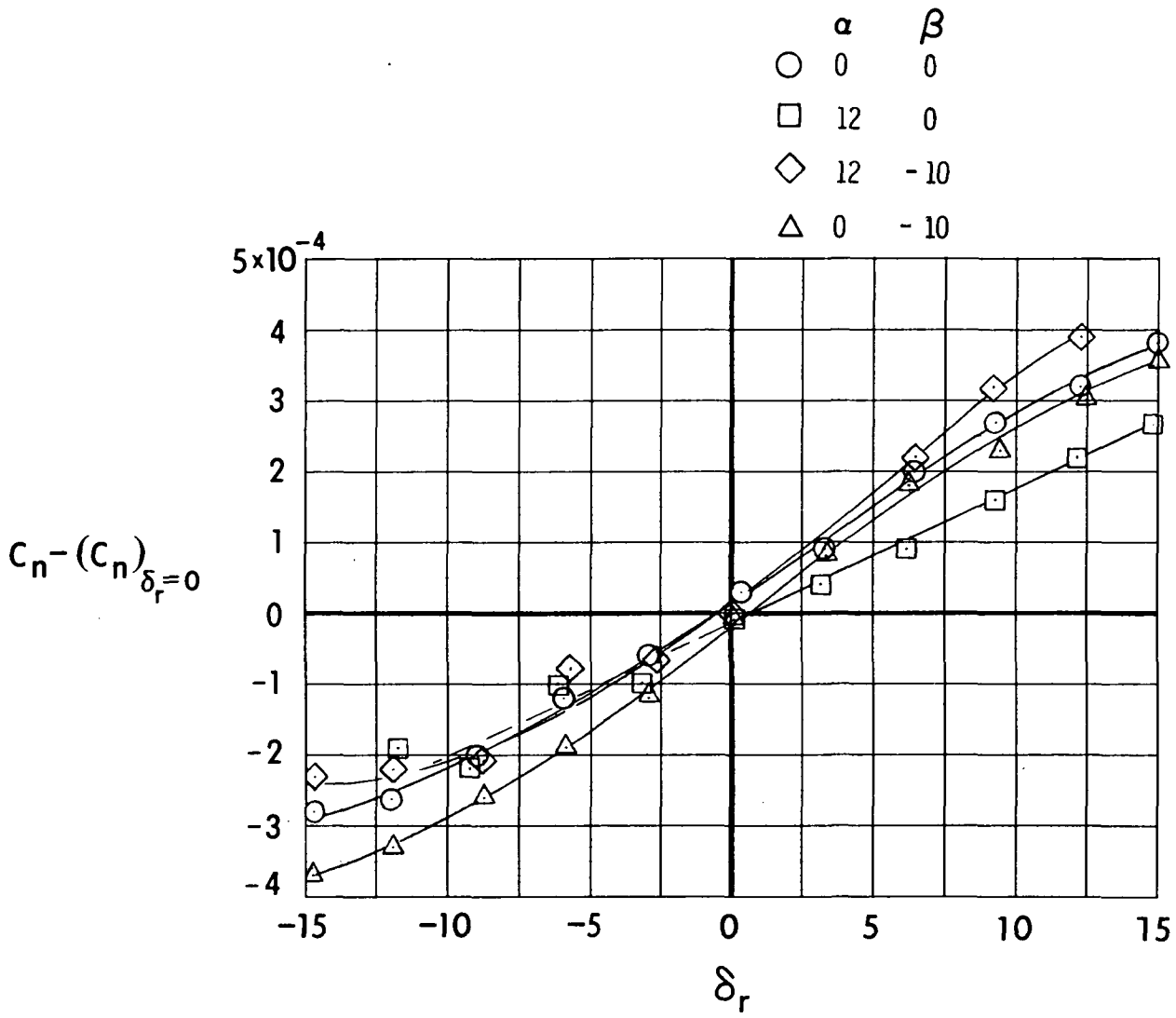

Figure 26.- Effect of rudder deflection on yawing-moment characteristics of model. Duct fins on.

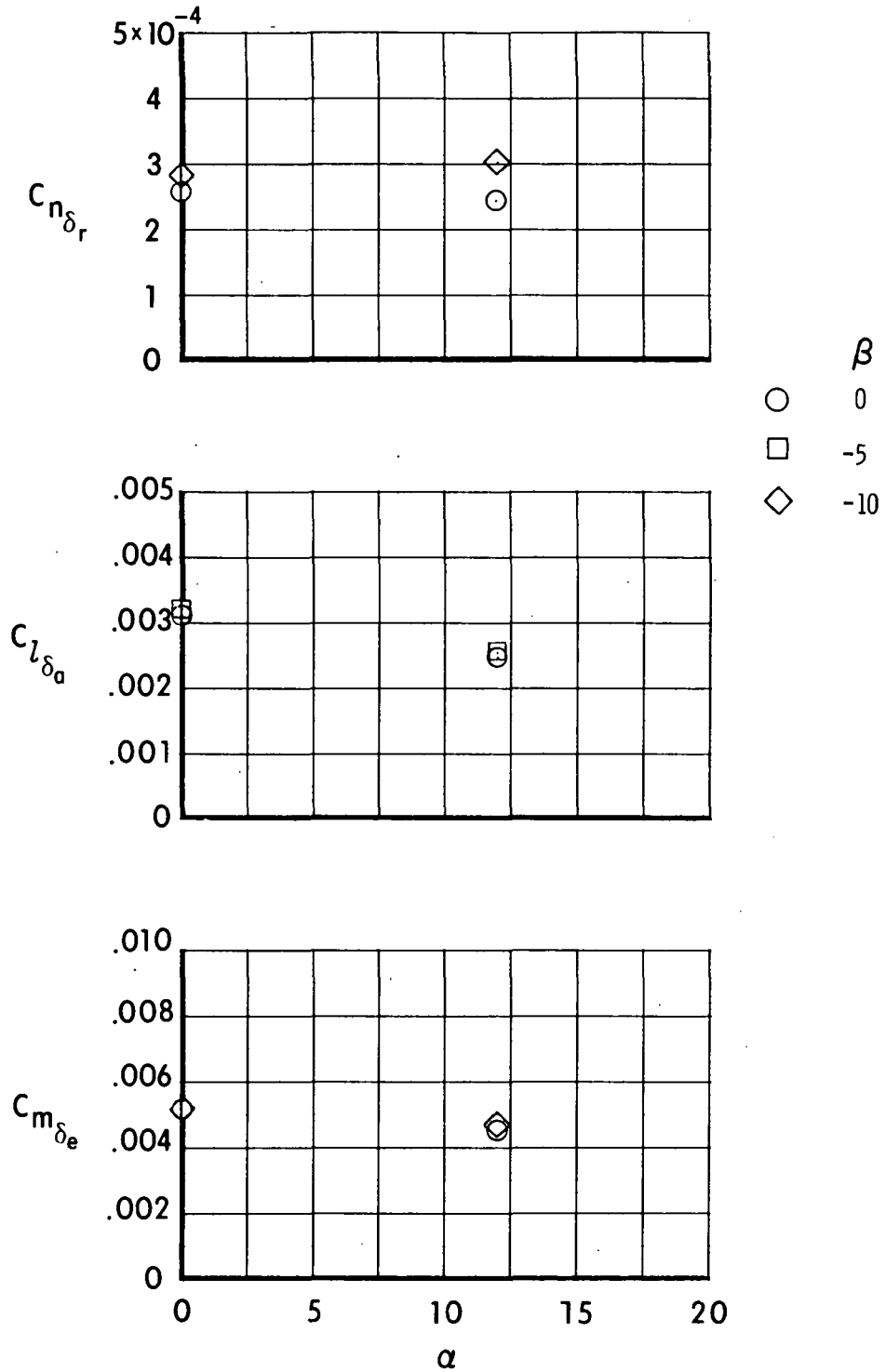

(a) $\delta_{d.b.} = 0^{o}$.

Figure 27.- Summary of aerodynamic control power.

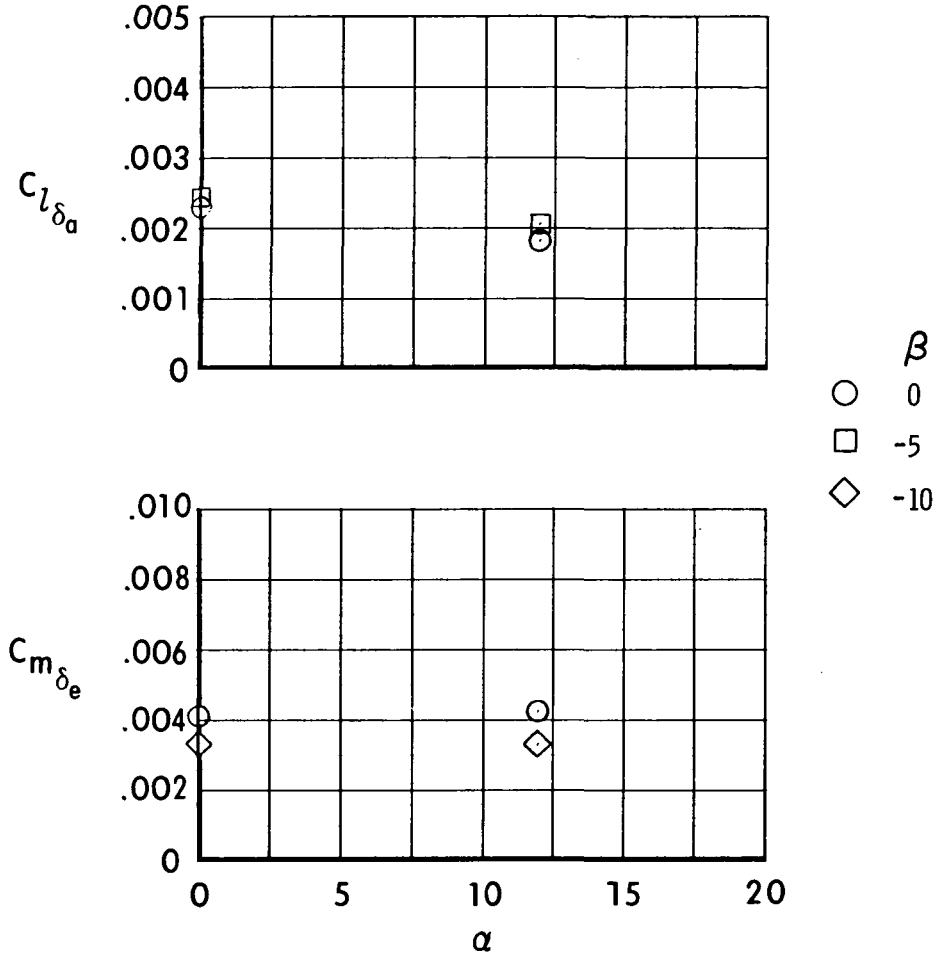

(b) $\delta_{d.b.} = 90^{o}$.

Figure 27.- Concluded.

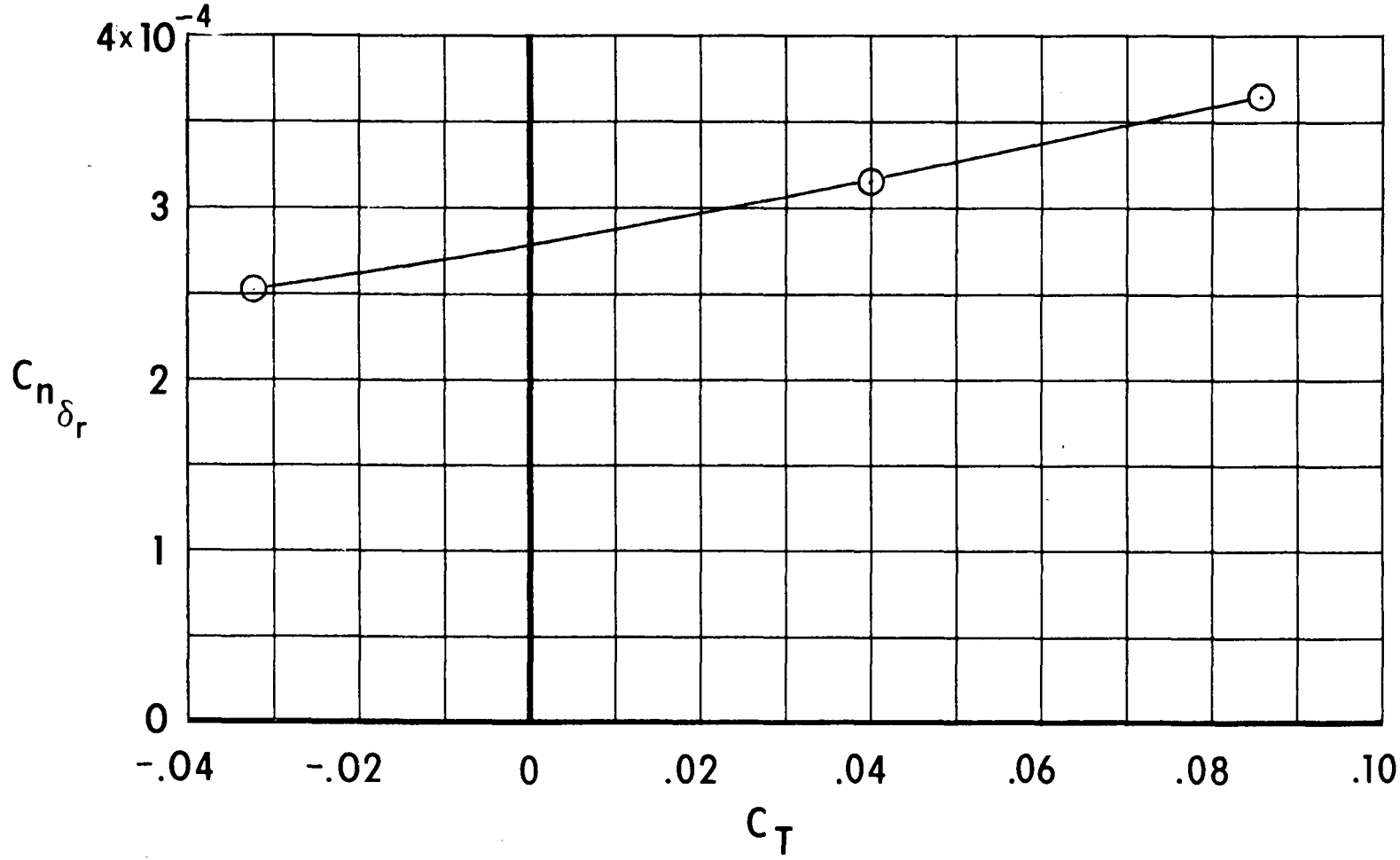

Figure 28.- Effect of power on directional control power.

1. Report No.	2. Government Accession No.	3. Recipient's Catalog No.
NASA TM-80132 AVRADCOM TR 79-41		

4. Title and Subtitle	5. Report Date
WIND-TUNNEL INVESTIGATION OF AN ARMED MINI REMOTELY PILOTED VEHICLE	September 1979
	6. Performing Organization Code

7. Author(s)	8. Performing Organization Report No.
Arthur E. Phelps III	L-13026
	10. Work Unit No. 505-10-23-05

9. Performing Organization Name and Address	11. Contract or Grant No.
Structures Laboratory AVRADCOM Research and Technology Laboratories NASA Langley Research Center Hampton, VA 23665	
	13. Type of Report and Period Covered: Technical Memorandum

12. Sponsoring Agency Name and Address	14. Army Project No.
National Aeronautics and Space Administration Washington, DC 20546 and U.S. Army Aviation Research and Development Command St. Louis, MO 63166	1L161102AH45

15. Supplementary Notes

Arthur E. Phelps III: Structures Laboratory, AVRADCOM Research and Technology Laboratories.

16. Abstract

A wind-tunnel investigation of a full-scale remotely piloted vehicle (RPV) armed with rocket launchers has been conducted in the Langley V/STOL tunnel. The results of the test indicate that the model had unacceptable longitudinal stability characteristics at negative angles of attack in the original design configuration. The addition of a pair of fins mounted in a V-arrangement on the propeller shroud resulted in a configuration with acceptable longitudinal stability characteristics. The addition of wing-mounted external stores to the modified configuration resulted in a slight reduction in the longitudinal stability. The lateral-directional characteristics of the model were generally good, but the model had low directional stability at low angles of attack. Aerodynamic control power was very strong around all three axes.

17. Key Words (Suggested by Author(s))	18. Distribution Statement
Remotely piloted vehicle (RPV) Strike RPV	Unclassified - Unlimited Subject Category 02

19. Security Classif. (of this report)	20. Security Classif. (of this page)	21. No. of Pages	22. Price*
Unclassified	Unclassified	59	$5.25

*For sale by the National Technical Information Service, Springfield, Virginia 22161

NASA-Langley, 1979

National Aeronautics and
Space Administration

Washington, D.C.
20546

Official Business
Penalty for Private Use, $300

THIRD-CLASS BULK RATE

Postage and Fees Paid
National Aeronautics and
Space Administration
NASA-451

U.S.MAIL

9 2 1U,A, 091179 S90844HU
MCDONNELL DOUGLAS CORP
ATTN: PUBLICATIONS GROUP PR 15246-A
P O BOX 516
ST LOUIS MO 63166

NASA

POSTMASTER: If Undeliverable (Section 158 Postal Manual) Do Not Return

27 MAR80 S Don Altken 341/336/600/23425 15 MAY 80 AC

9 SEP83 M Leonard Mockapetris E241/106/38158 15 AUG84 S

1987 MAY 18 Paul Dees 341/33/6/78/30743 AUG 28 1987

MAR 7 1988 Paul Dees 341/33/2/176/74322 JAN 15 1991

1200 5 OCT 1979